A SMAD1/5-YAP signaling module drives radial glial cell expansion and growth of the developing cerebral cortex

Sonia Najas[1,2], Isabel Pijuan[1,2], Anna Esteve-Codina[3], Susana Usieto[1], Juan D. Martinez[1], An Zwijsen[4], Mariona L. Arbonés[1,2], Elisa Martí[1] and Gwenvael Le Dréau[1,5,*]

[1] Department of Developmental Biology, Instituto de Biología Molecular de Barcelona, CSIC, Parc Científic de Barcelona, C/ Baldiri Reixac 10-15, 08028 Barcelona, Spain.

[2] Centro de Investigación Biomédica en Red de Enfermedades Raras (CIBERER), Barcelona, Spain.

[3] CNAG-CRG, Centre for Genomic Regulation (CRG), Barcelona Institute of Science and Technology (BIST), Baldiri i Reixac 4, 08028 Barcelona, Spain; Universitat Pompeu Fabra (UPF), Barcelona, Spain.

[4] Department of Cardiovascular Sciences, KU Leuven, Leuven 3000, Belgium.

[5] Lead contact

[*] Corresponding author: gldbmc@ibmb.csic.es

Key words: cerebral cortex; neurogenesis; radial glial cells; intermediate progenitor cells; Bone morphogenetic proteins (BMPs); SMAD transcription factors; YAP; cortical projection neurons.

Characters count (From title to Figure legends): 39,462

Summary

Cerebral cortex expansion in development and evolution is defined by the spatiotemporal production of neurons. Although the intracellular mechanisms regulating the decision of radial glial cells (RGCs) to self-amplify or produce neurons are beginning to be deciphered, the upstream signalling pathways involved are less well understood. Here we highlight an evolutionarily conserved role of the canonical BMP pathway in controlling neurogenesis and growth during corticogenesis. Through gain- and loss-of-function experiments on chick embryos, we found that the activity of the BMP effectors SMAD1/5 supports RGC self-amplification and impedes their premature differentiation and exhaustion. The microcephaly and overall growth retardation observed in conditional Smad1/5$^{wt/fl}$;Nestin:Cre$^{+/0}$ (SmadNes) mutant mice reveal this role to be evolutionarily conserved. Furthermore, we demonstrate that the effect of SMAD1/5 on RGCs depends on the activity of the Hippo signaling effector YAP. We anticipate this SMAD1/5-YAP signaling module to be fundamental in controlling growth and evolution of the amniote cerebral cortex.

Introduction

The cerebral cortex is the region of the human brain responsible for higher cognitive functions. Errors during its formation provoke a vast array of brain disorders that affect intellectual ability and social behaviour (Hu et al., 2014; Jayaraman et al., 2018). This highlights the relevance of identifying the mechanisms that govern cortical development, in particular those controlling its growth and the production of neurons from cortical stem and progenitor cells.

Emerging in the dorsal part of the telencephalon (pallium), the mammalian cerebral cortex first consists of a pseudo-stratified epithelial layer (also called the ventricular zone, VZ) formed by primitive neural stem cells, the neuroepithelial cells that mature into radial glial cells (RGCs) at the onset of neurogenesis (Taverna et al., 2014). Like neuroepithelial cells, RGCs contact both the ventricle and the basal lamina, they divide at the apical membrane and they can expand through self-amplifying divisions that produce two daughter RGCs (De Juan Romero and Borrell, 2015; Taverna et al., 2014). Neurogenesis can occur directly, whereby a RGC divides asymmetrically to generate another RGC and a daughter cell that differentiates directly into a neuron (De Juan Romero and Borrell, 2015; Taverna et al., 2014). Alternatively, neurogenesis can be indirect whereby a RGC gives rise to a RGC and a basal progenitor (BP) that harbours a restricted lineage potential, delaminates from the VZ and divides basally. These BPs will increase neuronal output, possibly self-amplifying for several rounds of divisions before generating two neurons through a final self-consuming division (Lui et al., 2011). While intermediate progenitor cells (IPCs) possess a very limited self-amplification potential and represent the vast majority of cortical BPs in lissencephalic species, basal (or outer) RGCs harbour a considerable self-amplification potential and they are responsible for the tremendous production of neurons and the larger neocortex

observed in gyrencephalic species (Lui et al., 2011; Shitamukai et al., 2011; Wang et al., 2011). Therefore, the decision of a RGC to self-amplify or to give rise to neurons, either directly or indirectly, has a huge impact on the final number of neurons in the cerebral cortex.

As highlighted by the genes whose mutation causes primary microcephaly, a variety of intracellular events regulate cerebral cortical size, including centrosome behaviour and centriole biogenesis, DNA replication and repair, cytokinesis and apical-basal polarity (Jayaraman et al., 2018; Saade et al., 2018). Moreover, the balance between RGC self-amplification and neurogenesis appears to be instructed by extrinsic cues emanating from the ventricular fluid, meninges, blood vessels and neighbouring cells (Llinares-Benadero and Borrell, 2019; Martynoga et al., 2012; Taverna et al., 2014). Thus, the molecular events regulating RGC fate are complex and they are still not fully understood.

Here, we studied the role of Bone morphogenetic protein (BMP) signalling in RGC fate decision during cortical development. The microcephaly described in *Bmp7* mutant mice, and the over-proliferation and premature differentiation reported in the brains of transgenic mice expressing a constitutively active form of the type-1 BMP receptors *Alk3/Bmpr1a* or *Alk6/Bmpr1b* (Panchision et al., 2001; Segklia et al., 2012), argue that BMP signaling is crucial for brain growth. Studies performed on cortical progenitors *in vitro* (Li et al., 1998; Mabie et al., 1999), and the ability of BMPs to promote self-expanding divisions during spinal neurogenesis (Le Dreau et al., 2014), further suggest an instructive role for BMP signaling in RGC fate decisions.

Here we found that the activity of the canonical BMP effectors SMAD1/5 is required for cortical RGC self-amplification in both chick and mouse embryos, preventing their premature neurogenic switch and exhaustion, and thereby ensuring the appropriate

production of the distinct classes of cortical excitatory neurons. In searching for the effectors of SMAD1/5 activity, we show that this role depends on the post-transcriptional regulation of YAP, a core component of the Hippo signaling pathway known to regulate cell growth and organ size (Yu et al., 2015). Together, our findings reveal an instructive and evolutionarily conserved role of the canonical BMP pathway in the control of RGC self-amplification, and in the growth of the developing cerebral cortex.

Results

SMAD1/5 activity is required for RGC self-amplification during chick cortical neurogenesis

To determine the role of the canonical BMP pathway during cerebral cortex development in amniotes, we focused on SMAD1/5/8. There is increasing evidence that the basic gene regulatory networks, progenitor cell types and cellular events governing the neuron generation during corticogenesis are evolutionarily conserved between mammals and sauropsids, particularly birds (Cardenas et al., 2018; Le Dreau et al., 2018; Nomura et al., 2013; Suzuki et al., 2012; Yamashita et al., 2018). Thus, we first assessed the role of these SMADs in the chick. The production of neurons in the PAX6^{+} developing chick cerebral cortex spans from embryonic days (E)3 to E8 (Figures 1A and S1A; Suzuki et al., 2012). As in mammals (Taverna et al., 2014), cortical neurogenesis in the chick is initiated by the onset of asymmetric neurogenic divisions of PAX6^{+};TBR2^{-} RGCs that divide apically in the VZ (Figures 1A,B and S1A-C). From E5 onwards, the production of cortical neurons is enhanced by symmetric neurogenic divisions of basally dividing TBR2^{+} IPCs (Figures 1A,B and S1A,C; Suzuki et al.,2012). *In situ* hybridization revealed that both *cSmad1* and *cSmad5* transcripts are expressed throughout this neurogenic period, mostly in the VZ where *cSmad8* transcripts were essentially absent (Figure S1D). Immunostaining with an antibody that specifically recognizes the active, carboxy-terminal phosphorylated form of SMAD1/5/8 (pSMAD1/5/8) revealed activity of these canonical BMP effectors in both apically- and basally-dividing cortical progenitors as well as in differentiating neurons (Figure 1C). When quantified in pH3^{+} mitotic nuclei, SMAD1/5 activity was weaker in basal IPC divisions than in RGC divisions (Figure 1D). When quantified after *in ovo* electroporation of a pTis21:RFP reporter that is specifically activated during neurogenic

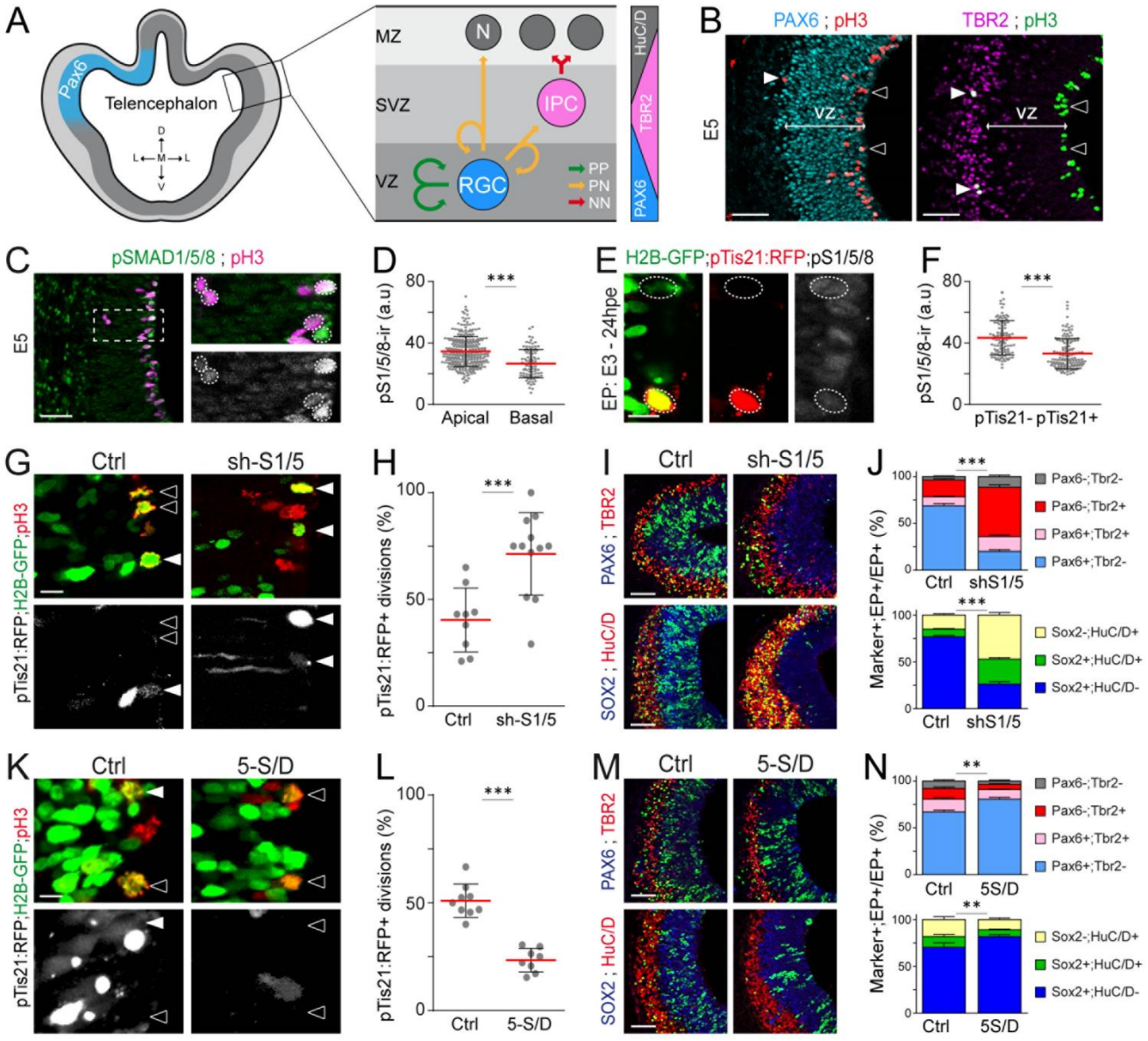

Figure 1: SMAD1/5 activity is required for RGC self-amplification during chick cortical neurogenesis.
(A) Cortical neurogenesis in the chick, showing the main cortical progenitor subtypes and their modes of division. (B) Chick PAX6+;TBR2- RGCs and TBR2+ IPCs undergo pH3+ mitoses apically (black arrowheads) and basally (white arrowheads) to the VZ, respectively. (C) The active, phosphorylated form of SMAD1/5/8 (pSMAD1/5/8) immunoreactivity at E5, and (D) its mean intensity ± s.d measured in 276 apical and 93 basal mitoses obtained from 5 embryos. (E) The pSMAD1/5/8 immunoreactivity in mitotic cortical progenitors 24 hours after in ovo electroporation (IOE) with the pTis21:RFP reporter along with a control H2B-GFP-producing plasmid, and (F) its mean intensity ± s.d quantified in 137 pTis21:RFP+ neurogenic divisions and 107 pTis21:RFP- self-amplifying divisions derived from 8 electroporated embryos. (G-N) The mean proportion ± s.d of electroporated (H2B-GFP+) cortical progenitors undergoing neurogenic pTis21:RFP+ divisions (white arrowheads) after IOE of shRNA plasmids targeting cSmad1 or cSmad5 (sh-S1/5) or their control (G, H) or IOE of a constitutively active SMAD5 mutant (5-S/D) or its control (K, L), obtained from 8-12 embryos per experimental condition. The mean proportion ± s.d of PAX6+/-;TBR2+/- and SOX2+/-;HuC/D+/- cells among electroporated (H2B-GFP+) cells 48 hours after IOE of sh-S1/5 (I, J), 5-S/D (M, N) or their respective controls, obtained from 8-20 embryos per experimental condition. Significance was assessed with the non-parametric Mann–Whitney test (D, F), the two-sided unpaired t-test (H, L) or a two-way ANOVA + Sidak's test (J, N). *P<0.05, **P<0.01, ***P<0.001. Scale bars: 50 µm (B, C, I, M), 10 µm (E, G, K). VZ: ventricular zone. See also Figures S1 and S2.

divisions (Figure S1E-G; Le Dreau et al., 2014; Saade et al., 2017; Saade et al., 2013), SMAD1/5 activity was diminished in pTis21:RFP^{+} neurogenic divisions relative to pTis21:RFP^{-} self-amplifying divisions (Figure 1E,F). Therefore, a positive correlation exists between SMAD1/5 activity and the potential for RGC self-amplification during chick cortical neurogenesis.

Endogenous SMAD1/5 activity was inhibited from the onset of cortical neurogenesis by *in ovo* electroporation of sh-RNA plasmids that specifically target *cSmad1* or *cSmad5* (sh-S1/5; Le Dreau et al., 2012). Inhibiting SMAD1/5 activity nearly doubled the proportion of electroporated RGCs undergoing neurogenic pTis21:RFP^{+} divisions (Figure 1G,H). This precocious switch to neurogenic divisions, equally caused by either SMAD1 or SMAD5 inhibition, provoked a premature depletion of electroporated PAX6^{+};TBR2^{-} RGCs, their accelerated progression towards a committed TBR2^{+} fate and ultimately, their differentiation into SOX2^{-};HuC/D^{+} and TBR1^{+} neurons (Figures 1I,J and S2A-H). Conversely, enhancing canonical BMP activity through *in ovo* electroporation of a constitutively active SMAD5 mutant (SMAD5-S/D; Le Dreau et al., 2012) produced the opposite phenotype, a 2-fold reduction in the proportion of electroporated RGCs undergoing neurogenic pTis21:RFP^{+} divisions (Figure 1K,L). This reduction in neurogenic divisions was associated with the electroporated cells remaining as PAX6^{+};TBR2^{-} RGCs and it impeded their transition into the neuronal lineage (Figure 1M,N). Notably, the SMAD5-S/D construct rescued the phenotype caused by sh-S5 (Figure S2I,J). In 5 out of 20 electroporated embryos, SMAD5-S/D electroporation itself caused the abnormal generation of ectopic rosettes of cortical progenitors, which developed an apical-basal polarity (Figure S2K). Together, these data identify a new role for SMAD1/5 in regulating cortical neurogenesis during chick development,

whereby the fine tuning of SMAD1/5 activity is required to properly balance the self-amplification of RGCs with the production of cortical excitatory neurons.

SMAD1/5 activity is required for RGC self-amplification and growth of the mouse cerebral cortex

We next assessed whether this function of SMAD1/5 is conserved during neurogenesis in the mammalian cerebral cortex. Unlike *mSmad8*, *mSmad1* and *mSmad5* transcripts are clearly expressed throughout the rostral-caudal axis of the developing mouse cerebral cortex at E14.5, and they are particularly enriched in the VZ (Figure 2A). As in chick embryos, pSMAD1/5/8 immunostaining revealed SMAD1/5 activity to be stronger in apically dividing mouse RGCs than in basally dividing IPCs (Figure 2B,C), suggesting a conservation of their role in maintaining cortical RGCs. To further understand the role played by SMAD1/5 during mouse cerebral cortex development, we crossed *Smad1*$^{fl/fl}$*;Smad5*$^{fl/fl}$ mice with a *Nestin:cre* transgenic line that produces Cre-mediated recombination in neural progenitor cells and somites as early as E8.5 (Moya et al., 2012; Petersen et al., 2002). Both SMAD1 and SMAD5 protein levels were reduced by ≈50% in E11.5 Smad1$^{wt/fl}$;Smad5$^{wt/fl}$;Nestin:Cre$^{+/0}$ embryos (hereafter referred to as SmadNes mutants or +/-) relative to their control Smad1$^{wt/fl}$;Smad5$^{wt/fl}$;Nestin:Cre$^{0/0}$ littermates (Figure S3A,B). The SmadNes mutant mice were viable, born following Mendelian ratios and sterile. From their early postnatal days to adulthood the SmadNes mutants were smaller and ≈30% lighter than their control littermates (Figure 2D,E), revealing severe growth retardation. Interestingly, the SmadNes mutants were microcephalic and while their brain/body weight ratio was higher at P7, it had recovered to normal levels by adulthood (Figure 2F-H), a characteristic reminiscent of human primordial dwarfism syndromes (Klingseisen and Jackson, 2011). The size reduction of

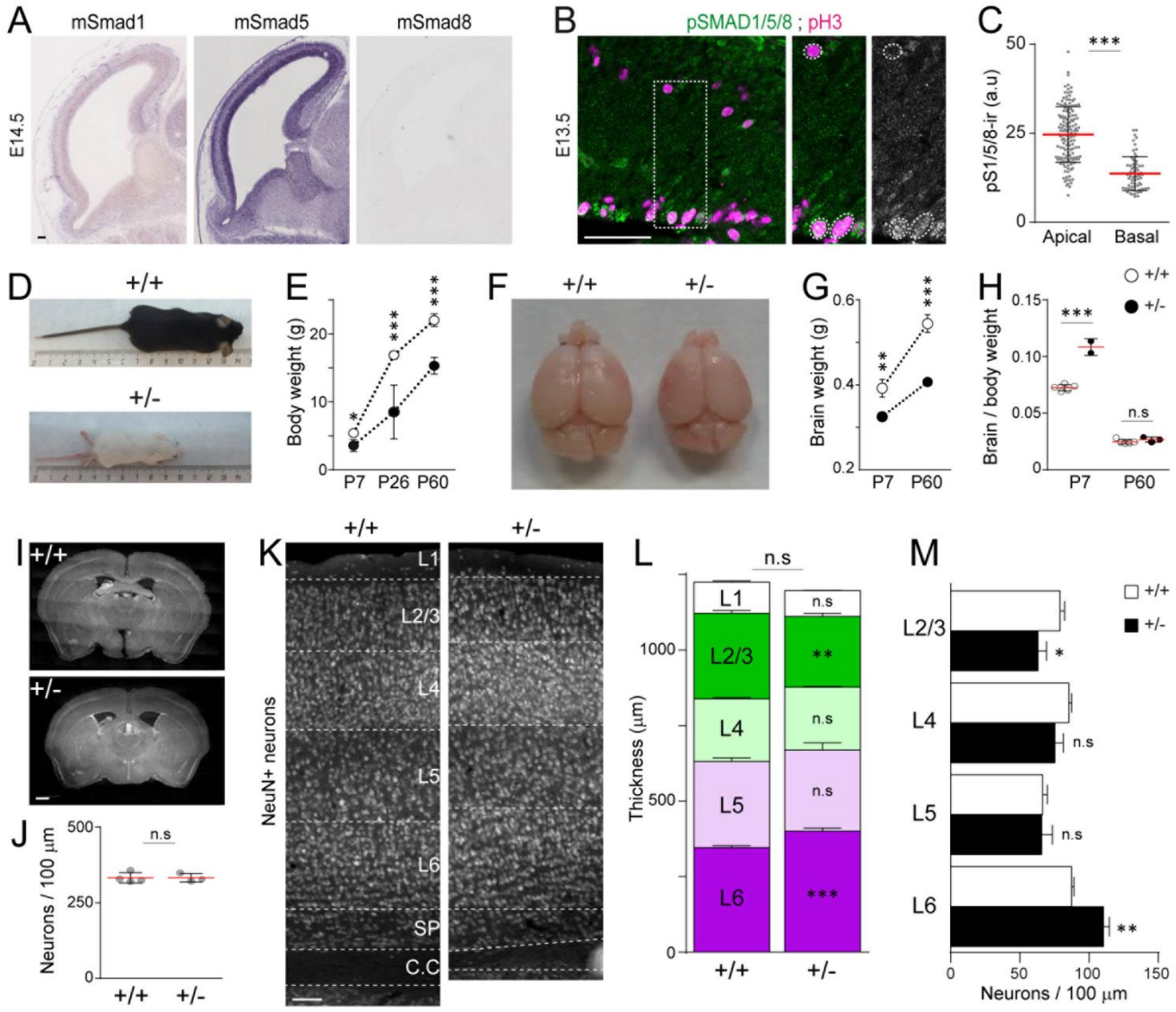

Figure 2: inhibiting SMAD1/5 activity in mouse neural progenitors causes growth retardation, microcephaly and cortical alterations.
(A) Sagittal sections of the developing mouse dorsal telencephalon showing mSmad1, mSmad5 and mSmad8 transcripts at E14.5, obtained from Genepaint (https://gp3.mpg.de). (B) The pSMAD1/5/8 immunoreactivity at E13.5 and (C) its mean intensity ± s.d measured in 144 apical and 64 basal mitoses obtained from 3 embryos. (D-H) The postnatal evolution of SmadNes mutant mice and their control littermates (D) in terms of mean postnatal weight ± s.d (E), brain development (F), mean brain weight ± s.d (G) and the brain/body weight ratio ± s.d (H), obtained from 3-12 animals per genotype. (I) Coronal sections of the brain of adult SmadNes mutant mice and their control littermates. (J-L) Mean number of NeuN+ neurons ± s.d (J), neuronal layer organization (K), mean thickness of the layers ± s.d (L) and the mean number of neurons ± s.d in the different layers (M) in radial units (100 µm) of the mature cerebral cortex of SmadNes mutant mice and their control littermates, obtained from 3-4 animals per genotype. Significance was assessed with the non-parametric Mann–Whitney test (C, J) or a two-way ANOVA + Sidak's test (E, G, H, L, M). *P<0.05, **P<0.01, ***P<0.001. Scale bars, 50 µm (B), 100 µm (A, K), 500 µm (I). See also Figure S3.

the adult SmadNes mutant brain was constant across the rostral-caudal axis (Figure S3C,D), suggesting that SMAD1/5 inhibition impaired growth equally in all brain regions. Apart from these growth defects and a thinner corpus callosum, the brain of the SmadNes mutants did not present any major neuro-anatomical defects (Figures 2I and S3C-E). Intriguingly, the neocortex of adult SmadNes mutants did not appear to have fewer neurons per radial column unit but the relative proportions of its neuronal layers were altered (Figure 2J-M). The number of early-born neurons forming the deep layer L6 and its thickness increased, whereas these parameters diminished in the superficial L2/3 layer containing late-born callosal projection neurons, consistent with the reduced thickness of the corpus callosum (Figures 2K-M and S3E). This phenotype was observed at P7 (Figure S3F-J), supporting the idea that these cortical defects originated during the embryonic phase.

While the SmadNes mutant embryos did not present any obvious defect in telencephalic patterning (Figure S4A,B), their programme of cortical neurogenesis did appear to be altered (Figure 3). Around the onset of cortical neurogenesis (E11.5), the SmadNes mutant embryos had correct numbers of RGCs ($PAX6^+$;$TBR2^-$ cells) and IPCs ($TBR2^+$ cells) per radial unit, yet their neuronal output was increased (Figure 3A-F). Accordingly, there were more early-born differentiating $TBR1^+$ neurons in the SmadNes mutant cortex than in their control littermates from E11.5 onwards (Figure 3G,H). The developing cerebral cortex of the SmadNes mutant embryos contained fewer IPCs from E13.5 onwards and fewer RGCs at E17.5 (Figure 3B-D). This decrease in cortical progenitors at E17.5 was associated with a lower neuronal output and fewer late-born $SATB2^+$ neurons (Figure 3E,F and I,J). The mitotic indices of the cortical RGCs and IPCs were comparable in SmadNes mutants and controls at all stages examined (Figure S4C-E), indicating that the alterations to cortical neurogenesis in

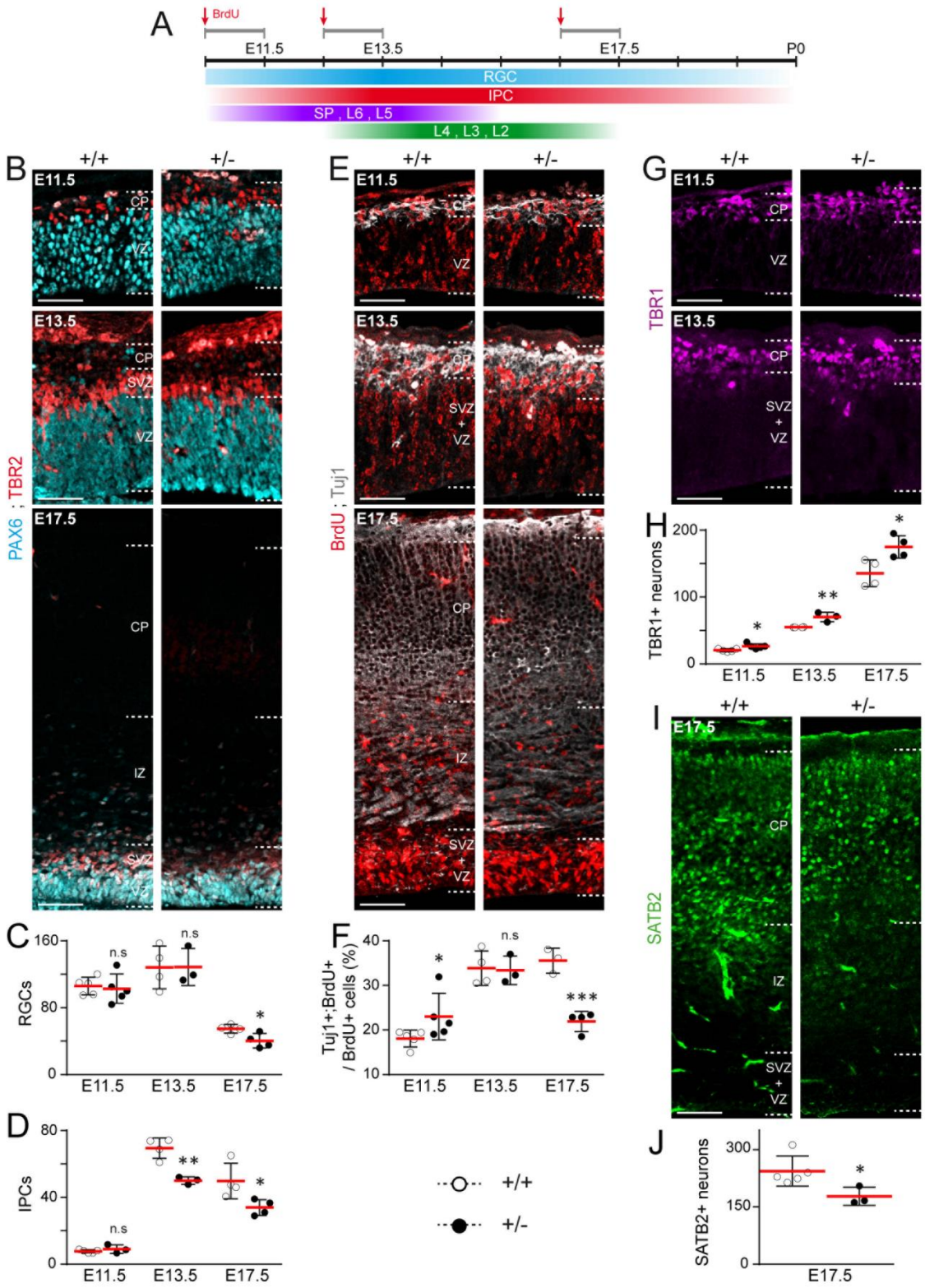

Figure 3: inhibiting SMAD1/5 activity in mouse cortical progenitors causes premature neurogenesis, and depletion of the RGC and IPC pools.

(A) Timeline of cortical neurogenesis and BrdU injections during mouse embryonic development. (B-J) Immunostaining and quantification of the mean numbers ± s.d. of PAX6+;TBR2- RGCs and TBR2+ IPCs (B-D), the neuronal output (% of BrdU+; Tuj1+/BrdU+ cells, E, F), the generation of early-born TBR1+ (G, H) and late-born SATB2+ (I, J) cortical excitatory neurons quantified per radial unit (100 µm) in the developing cerebral cortex of SmadNes mutant mice and their control littermates at early (E11.5), middle (E13.5) and late (E17.5) embryonic stages, obtained from 3-5 embryos per genotype and stage. The normality was tested using the values of individual sections. Significance was assessed with the two-sided unpaired t-test (C, D, F, H, J). *P<0.05, **P<0.01, ***P<0.01. Scale bars, 50 µm. CP: cortical plate, IZ: intermediate zone, SVZ: sub-ventricular zone, VZ: ventricular zone. See also Figure S4.

SmadNes mutants are not the result of altered cell cycle kinetics. Together, these data confirmed the developmental origin of the cortical alterations seen in the cerebral cortex of the adult SmadNes mutants (Figure 2K-M). They moreover reveal that mouse cortical progenitors with weaker SMAD1/5 activity prematurely switch to neurogenic divisions, enhancing the generation of early-born cortical neurons and prematurely exhausting the RGC and IPC pools. Consequently, the production of late-born cortical neurons is limited. As such, the role of SMAD1/5 in promoting RGC maintenance appears to be conserved in mammalian corticogenesis.

SMAD1/5 regulate RGC self-amplification and early cortical neurogenesis through YAP

To identify the gene regulatory networks controlled by SMAD1/5 during cortical neurogenesis, cortical RGCs from SmadNes mutant and control E12.5 embryos were purified by FACS based on their Prominin1 expression (Corti et al., 2007), and their transcriptomes were compared by genome-wide RNA-sequencing (Figure 4A). A short list of differentially expressed transcripts (DETs) was identified (90 DETs with adj $p<0.05$ and 128 with adj $p<0.1$: Figure 4B and Table S1). A gene ontology (GO) term enrichment analysis correlated this DET signature to the regulation of neurogenesis and cell biosynthesis (Figure 4C). A Transfac/Jaspar analysis revealed that the promoter regions of these DETs are enriched in binding motifs for transcription factors of the TEAD and SP families (Figure 4D). The activity of TEADs depends directly on the availability of their co-factors YAP/TAZ (Yu et al., 2015). YAP/TAZ are themselves regulated by various upstream signals, including the IGF and Hippo signalling pathways that regulate cell growth and organ size, and the deregulation of which has been linked to primordial dwarfism syndromes (Klingseisen and Jackson, 2011; Yu et al., 2015).

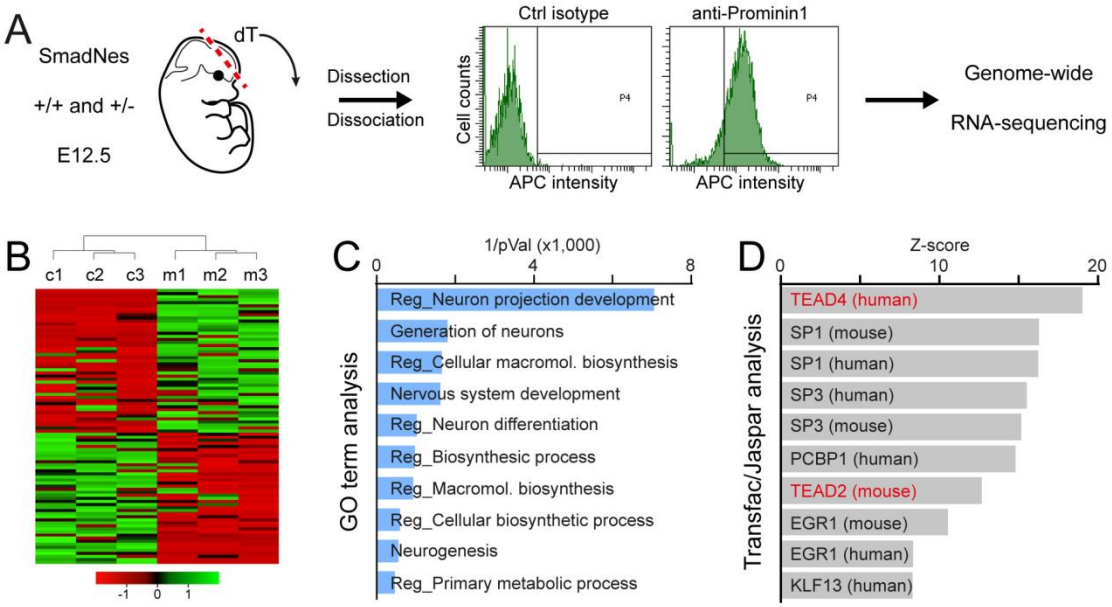

Figure 4: Transcriptional program regulated by SMAD1/5 in early mouse cortical RGCs.
(A) Methodology used to compare the transcriptome of cortical RGCs from SmadNes mutant and control E12.5 embryos. (B) Spearman rank correlation and heatmap representing the differentially expressed transcripts (DETs, with a pAdj<0.05) between mutant and control cortical RGCs. (C, D) Representation of the top 10 gene ontology biological processes (C) and transcription factor binding motifs (D) associated with the DETs (with a pAdj<0.1). See also Table S1.

Remarkably, SMAD1/5 and YAP may interact physically and act synergistically (Alarcon et al., 2009; Huang et al., 2016).

Therefore, we analysed YAP expression and activity relative to SMAD1/5 activity during cortical neurogenesis (Figure 5). In agreement with recent reports (Kostic et al., 2019; Saito et al., 2018), immunostaining for the YAP protein revealed that the active (nuclear) YAP was more intensely expressed in apically-dividing RGCs than in basally-dividing IPCs, and its expression was strongly correlated with SMAD1/5 activity during both chick and mouse cortical neurogenesis (Figures 5A-D and S5A-D). Inhibiting SMAD1/5 during chick cortical neurogenesis impaired YAP activity, as witnessed through the reduced nuclear YAP intensity and the increase in the phosphorylated form of YAP (pYAP) primed for proteasomal degradation relative to the total YAP (Figures 5E,F and S5E,F). Similarly, the pYAP/YAP ratio increased in the cortex of E11.5 SmadNes mutant embryos (Figures 5G,H and S5G,H). These latter findings indicate that SMAD1/5 control YAP activity both during mouse and chick cortical neurogenesis.

Finally, we tested whether increasing YAP activity could compensate for the phenotype caused by SMAD1/5 inhibition. *In ovo* electroporation of a wild type form of YAP rescued the premature exhaustion of RGCs, reverting this to control levels and impeding their differentiation into $SOX2^{-}$;HuC/D^{+} neurons driven by sh-S1 (Figures 5I-L). Intriguingly, YAP overexpression forced the vast majority of electroporated cells to remain $SOX2^{+}$ (Figure 5I,J), with more than 30% being found ectopically in the mantle zone irrespective of SMAD1 inhibition (Figures 5I,M and S5I). Together, these results indicate that YAP is a key factor through which SMAD1/5 act to promote RGC self-amplification and orchestrate cortical neurogenesis and growth.

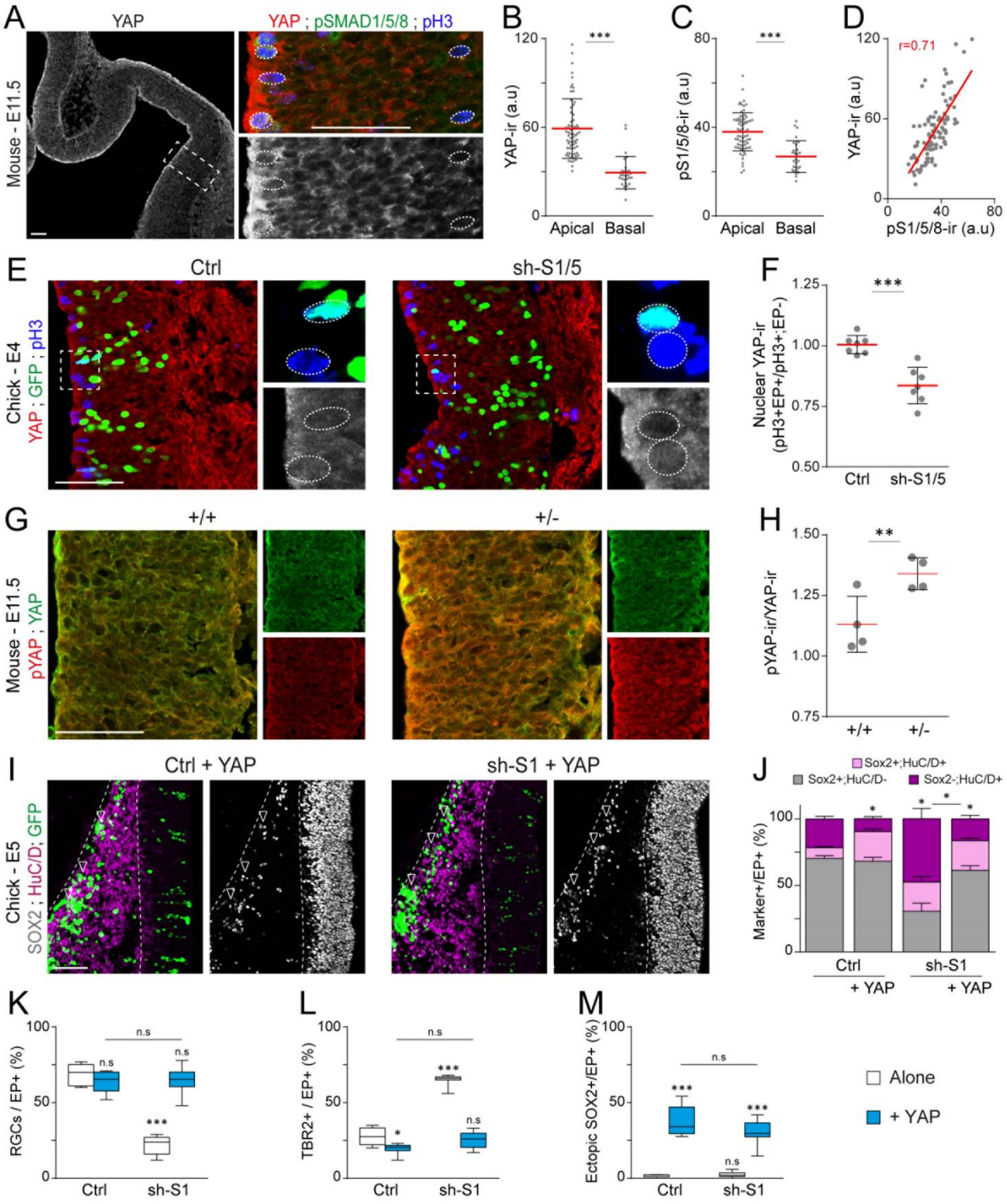

Figure 5: SMAD1/5 regulate early cortical neurogenesis through YAP.
(A) Expression of YAP during early mouse corticogenesis (E11.5), relative to SMAD1/5 activity (pSMAD1/5/8). (B,C) The mean intensity ± s.d. of endogenous YAP (B) and pSMAD1/5/8 (C) immunoreactivity was quantified in 70 apical and 28 basal pH3+ mitotic nuclei, obtained from 3 embryos. (D) The correlation between the intensity of endogenous pSMAD1/5/8 and YAP immunoreactivities was assessed by calculating the Pearson's correlation coefficient r. (E) Immunostaining of the developing chick cerebral cortex for total YAP 24 hours after IOE with a control or sh-S1/5 plasmid and (F) its mean ratio ± s.d. quantified in electroporated relative to non-electroporated mitotic cells obtained from 7 embryos (Ctrl: 147 pH3+;GFP+ cells and 154 pH3+;GFP- cells, sh-S1/5: 162 pH3+;GFP+ cells and 140 pH3+;GFP- cells). (G) Immunostaining of pYAP and total YAP and (H) the quantification of the pYAP/YAP intensity ratio ± s.d. in the developing cerebral cortex of E11.5 SmadNes mutant embryos and control littermates, obtained from 4 embryos (12 sections) per genotype. The normality was tested using the values of individual sections. (I-M) Immunostaining and the mean proportion ± s.e.m. of SOX2+/-;HuC/D+/- cells (I, J), RGCs (PAX6+;TBR2- cells, K), TBR2+ cells (L) and ectopic SOX2+ cells (M) among electroporated (GFP+) cells 48 hours after IOE of a wild type YAP1 construct (YAP) together with sh-S1 or its control, obtained from n=8-9 embryos per condition. Significance was assessed with the non-parametric Mann–Whitney test (B, C, F), the two-sided unpaired t-test (H) or a two-way ANOVA + Tukey's multiple comparisons test (J-M). *P<0.05, **P<0.01, ***P<0.001. Scale bars, 50 µm. See also Figure S5.

Discussion

In this study, we identify a role for the canonical BMP effectors SMAD1/5 in cortical neurogenesis, whereby their activity is required for RGC self-amplification. Indeed, SMAD1/5 prevent the premature neurogenic switch and exhaustion of cortical progenitor cells, ensuring the appropriate production of the distinct classes of cortical excitatory neurons. Alteration of this SMAD1/5 activity is likely to underlie the microcephaly described in *Bmp7* mutant mice and the phenotype of excess proliferation in mice overexpressing a constitutively active form of the type-1 receptor *Alk3* (Panchision et al., 2001; Segklia et al., 2012). Notably, the cerebral cortex of adult SmadNes mutant mice is smaller along the medial-lateral and rostral-caudal axes, although its thickness and the number of neurons in the radial columns are nearly normal. These observations suggest that reducing SMAD1/5 activity more severely affects the generation of radial columns than the number of cells per radial unit, emphasizing the importance of SMAD1/5 activity for cortical RGC self-amplification. Since SmadNes mutant mice present an overall reduction in brain size and weight, it is likely that SMAD1/5 play a similar role throughout the developing brain. Our previous demonstration that SMAD1/5 promote stemness during spinal neurogenesis (Le Dreau et al., 2014), further suggests that canonical BMP signalling through SMAD1/5 regulates stem cell maintenance and growth throughout the developing CNS.

Using the mouse and chick as models of mammalian and avian corticogenesis, we established that the dependence on SMAD1/5 activity to maintain RGC self-amplification and appropriate neuronal production during corticogenesis is evolutionarily conserved. This leads us to propose that canonical BMP signaling is part of the core ancestral gene regulatory network that governs corticogenesis throughout the amniote lineage, together with PAX6, the proneural bHLH proteins and the Notch and

Slit/Robo signalling pathways (Cardenas et al., 2018; Le Dreau et al., 2018; Nomura et al., 2013; Suzuki et al., 2012; Yamashita et al., 2018).

The crucial role of SMAD1/5 in growth control during CNS development is further supported by our data showing that SMAD1/5 regulate YAP activity in early cortical RGCs. As a central element in the Hippo signaling pathway, YAP plays a fundamental role in the control of cell growth and of organ size in many tissues (Yu et al., 2015). Accordingly, the tight regulation of YAP activity appears to be crucial for correct brain formation and growth. Cortical and general brain development is affected when YAP activity is enhanced, either directly or indirectly (Lavado et al., 2013; Lavado et al., 2018; Liu et al., 2018; Saito et al., 2018). More importantly, an aberrant increase in YAP activity has been linked to various types of cortical heterotopia, such as those observed in the Van Maldergem syndrome (Cappello et al., 2013; Liu et al., 2018). Our observation that YAP overexpression causes ribbon-like heterotopias of $SOX2^{+}$ and $PAX6^{+}$ progenitors in the developing chick cerebral cortex is therefore reminiscent of these severe mammalian cortical defects. Conversely, a reduction in YAP activity is plausibly one of the mechanistic events contributing to primordial dwarfism syndromes (Klingseisen and Jackson, 2011). Remarkably, several features of primordial dwarfism were observed in the SmadNes mutant mice, such as growth retardation, microcephaly and a normal adult brain/body weight ratio. Interestingly, YAP activity also determines the abundance and proliferative ability of neocortical basal progenitors (Kostic et al., 2019), such that its regulation might have contributed to the evolutionary diversification and expansion of the mammalian neocortex. As the regulation of YAP activity by SMAD1/5 in RGCs appears to be evolutionarily conserved, it is tempting to speculate that modulation of canonical BMP activity might have influenced the growth and expansion of the cerebral cortex during amniote evolution.

Acknowledgments

Acknowledgements: we thank the members of M.L.A's and E.M's laboratories for their discussion of this study. We thank E. Rebollo and the IBMB Molecular Imaging platform, J. Comas and the PCB Flow Cytometry facility, and the CNAG-CRG Sequencing Unit for their assistance. We are grateful to E.J. Robertson for providing the *Smad1*$^{fl/fl}$ mice. **Funding:** the work in M.L.A's and E.M's laboratories was supported by the grants SAF2013-46676-P, SAF2016-77971-R, BFU2016-81887-REDT and BFU2016-77498-P. I.P. received a PhD fellowship from the Spanish Ministry of Economy, Industry and Competitiveness (MINEICO, BES2014-069217). A. E-C was supported by ISCIII (MINEICO, PT17/0009/0019) and the Fondo Europeo de Desarrollo Regional (FEDER). G.L.D. was supported by the AECC (AIO2014). **Author contributions:** Conceptualization: S.N. and G.L.D.; Methodology: S.N., I.P., A.E-C., S.U., J.D.M. and G.L.D.; Investigation: S.N., I.P., A.E-C. and G.L.D.; Resources: A.Z., M.L.A and E.M; Visualization: G.L.D.; Writing - Original Draft: G.L.D.; Funding Acquisition: M.L.A. and E.M.; Supervision: M.L.A., E.M. and G.L.D. **Competing interests:** the authors have no competing financial interests to declare. **Data and materials availability:** All data is available in the main text or supplemental information. **Correspondence and requests for materials** should be addressed to G.L.D.

References

Alarcon, C., Zaromytidou, A.I., Xi, Q., Gao, S., Yu, J., Fujisawa, S., Barlas, A., Miller, A.N., Manova-Todorova, K., Macias, M.J., *et al.* (2009). Nuclear CDKs drive Smad transcriptional activation and turnover in BMP and TGF-beta pathways. Cell *139*, 757-769.

Cappello, S., Gray, M.J., Badouel, C., Lange, S., Einsiedler, M., Srour, M., Chitayat, D., Hamdan, F.F., Jenkins, Z.A., Morgan, T., *et al.* (2013). Mutations in genes encoding the cadherin receptor-ligand pair DCHS1 and FAT4 disrupt cerebral cortical development. Nat Genet *45*, 1300-1308.

Cardenas, A., Villalba, A., de Juan Romero, C., Pico, E., Kyrousi, C., Tzika, A.C., Tessier-Lavigne, M., Ma, L., Drukker, M., Cappello, S., *et al.* (2018). Evolution of Cortical Neurogenesis in Amniotes Controlled by Robo Signaling Levels. Cell *174*, 590-606 e521.

Corti, S., Nizzardo, M., Nardini, M., Donadoni, C., Locatelli, F., Papadimitriou, D., Salani, S., Del Bo, R., Ghezzi, S., Strazzer, S., *et al.* (2007). Isolation and characterization of murine neural stem/progenitor cells based on Prominin-1 expression. Exp Neurol *205*, 547-562.

Chen, E.Y., Tan, C.M., Kou, Y., Duan, Q., Wang, Z., Meirelles, G.V., Clark, N.R., and Ma'ayan, A. (2013). Enrichr: interactive and collaborative HTML5 gene list enrichment analysis tool. BMC Bioinformatics *14*, 128.

De Juan Romero, C., and Borrell, V. (2015). Coevolution of radial glial cells and the cerebral cortex. Glia *63*, 1303-1319.

Dobin, A., Davis, C.A., Schlesinger, F., Drenkow, J., Zaleski, C., Jha, S., Batut, P., Chaisson, M., and Gingeras, T.R. (2013). STAR: ultrafast universal RNA-seq aligner. Bioinformatics *29*, 15-21.

Hamburger, V., and Hamilton, H.L. (1951). A series of normal stages in the development of chick embryo. J Morphol *88*, 49-92.

Hu, W.F., Chahrour, M.H., and Walsh, C.A. (2014). The diverse genetic landscape of neurodevelopmental disorders. Annu Rev Genomics Hum Genet *15*, 195-213.

Huang, Z., Hu, J., Pan, J., Wang, Y., Hu, G., Zhou, J., Mei, L., and Xiong, W.C. (2016). YAP stabilizes SMAD1 and promotes BMP2-induced neocortical astrocytic differentiation. Development *143*, 2398-2409.

Jayaraman, D., Bae, B.I., and Walsh, C.A. (2018). The Genetics of Primary Microcephaly. Annu Rev Genomics Hum Genet *19*, 177-200.

Klingseisen, A., and Jackson, A.P. (2011). Mechanisms and pathways of growth failure in primordial dwarfism. Genes Dev *25*, 2011-2024.

Kojima, S., Vignjevic, D., and Borisy, G.G. (2004). Improved silencing vector co-expressing GFP and small hairpin RNA. Biotechniques *36*, 74-79.

Kostic, M., Paridaen, J., Long, K.R., Kalebic, N., Langen, B., Grubling, N., Wimberger, P., Kawasaki, H., Namba, T., and Huttner, W.B. (2019). YAP Activity Is Necessary and Sufficient for Basal Progenitor Abundance and Proliferation in the Developing Neocortex. Cell Rep *27*, 1103-1118 e1106.

Kuleshov, M.V., Jones, M.R., Rouillard, A.D., Fernandez, N.F., Duan, Q., Wang, Z., Koplev, S., Jenkins, S.L., Jagodnik, K.M., Lachmann, A., *et al.* (2016). Enrichr: a comprehensive gene set enrichment analysis web server 2016 update. Nucleic Acids Res *44*, W90-97.

Lavado, A., He, Y., Pare, J., Neale, G., Olson, E.N., Giovannini, M., and Cao, X. (2013). Tumor suppressor Nf2 limits expansion of the neural progenitor pool by inhibiting Yap/Taz transcriptional coactivators. Development *140*, 3323-3334.

Lavado, A., Park, J.Y., Pare, J., Finkelstein, D., Pan, H., Xu, B., Fan, Y., Kumar, R.P., Neale, G., Kwak, Y.D., *et al.* (2018). The Hippo Pathway Prevents YAP/TAZ-Driven Hypertranscription and Controls Neural Progenitor Number. Dev Cell *47*, 576-591 e578.

Le Dreau, G., Escalona, R., Fueyo, R., Herrera, A., Martinez, J.D., Usieto, S., Menendez, A., Pons, S., Martinez-Balbas, M.A., and Marti, E. (2018). E proteins sharpen neurogenesis by modulating proneural bHLH transcription factors' activity in an E-box-dependent manner. Elife *7*.

Le Dreau, G., Garcia-Campmany, L., Rabadan, M.A., Ferronha, T., Tozer, S., Briscoe, J., and Marti, E. (2012). Canonical BMP7 activity is required for the generation of discrete neuronal populations in the dorsal spinal cord. Development *139*, 259-268.

Le Dreau, G., Saade, M., Gutierrez-Vallejo, I., and Marti, E. (2014). The strength of SMAD1/5 activity determines the mode of stem cell division in the developing spinal cord. J Cell Biol *204*, 591-605.

Levy, D., Adamovich, Y., Reuven, N., and Shaul, Y. (2008). Yap1 phosphorylation by c-Abl is a critical step in selective activation of proapoptotic genes in response to DNA damage. Molecular cell *29*, 350-361.

Li, B., and Dewey, C.N. (2011). RSEM: accurate transcript quantification from RNA-Seq data with or without a reference genome. BMC Bioinformatics *12*, 323.

Li, W., Cogswell, C.A., and LoTurco, J.J. (1998). Neuronal differentiation of precursors in the neocortical ventricular zone is triggered by BMP. J Neurosci *18*, 8853-8862.

Liu, W.A., Chen, S., Li, Z., Lee, C.H., Mirzaa, G., Dobyns, W.B., Ross, M.E., Zhang, J., and Shi, S.H. (2018). PARD3 dysfunction in conjunction with dynamic HIPPO signaling drives cortical enlargement with massive heterotopia. Genes Dev *32*, 763-780.

Love, M.I., Huber, W., and Anders, S. (2014). Moderated estimation of fold change and dispersion for RNA-seq data with DESeq2. Genome Biol *15*, 550.

Lui, J.H., Hansen, D.V., and Kriegstein, A.R. (2011). Development and evolution of the human neocortex. Cell *146*, 18-36.

Llinares-Benadero, C., and Borrell, V. (2019). Deconstructing cortical folding: genetic, cellular and mechanical determinants. Nat Rev Neurosci.

Mabie, P.C., Mehler, M.F., and Kessler, J.A. (1999). Multiple roles of bone morphogenetic protein signaling in the regulation of cortical cell number and phenotype. J Neurosci *19*, 7077-7088.

Martynoga, B., Drechsel, D., and Guillemot, F. (2012). Molecular control of neurogenesis: a view from the mammalian cerebral cortex. Cold Spring Harb Perspect Biol *4*.

Megason, S.G., and McMahon, A.P. (2002). A mitogen gradient of dorsal midline Wnts organizes growth in the CNS. Development *129*, 2087-2098.

Moya, I.M., Umans, L., Maas, E., Pereira, P.N., Beets, K., Francis, A., Sents, W., Robertson, E.J., Mummery, C.L., Huylebroeck, D., *et al.* (2012). Stalk cell phenotype depends on integration of Notch and Smad1/5 signaling cascades. Dev Cell *22*, 501-514.

Nomura, T., Gotoh, H., and Ono, K. (2013). Changes in the regulation of cortical neurogenesis contribute to encephalization during amniote brain evolution. Nat Commun *4*, 2206.

Panchision, D.M., Pickel, J.M., Studer, L., Lee, S.H., Turner, P.A., Hazel, T.G., and McKay, R.D. (2001). Sequential actions of BMP receptors control neural precursor cell production and fate. Genes Dev *15*, 2094-2110.

Petersen, P.H., Zou, K., Hwang, J.K., Jan, Y.N., and Zhong, W. (2002). Progenitor cell maintenance requires numb and numblike during mouse neurogenesis. Nature *419*, 929-934.
Saade, M., Blanco-Ameijeiras, J., Gonzalez-Gobartt, E., and Marti, E. (2018). A centrosomal view of CNS growth. Development *145*.
Saade, M., Gonzalez-Gobartt, E., Escalona, R., Usieto, S., and Marti, E. (2017). Shh-mediated centrosomal recruitment of PKA promotes symmetric proliferative neuroepithelial cell division. Nat Cell Biol *19*, 493-503.
Saade, M., Gutierrez-Vallejo, I., Le Dreau, G., Rabadan, M.A., Miguez, D.G., Buceta, J., and Marti, E. (2013). Sonic hedgehog signaling switches the mode of division in the developing nervous system. Cell Rep *4*, 492-503.
Saito, K., Kawasoe, R., Sasaki, H., Kawaguchi, A., and Miyata, T. (2018). Neural Progenitor Cells Undergoing Yap/Tead-Mediated Enhanced Self-Renewal Form Heterotopias More Easily in the Diencephalon than in the Telencephalon. Neurochem Res *43*, 180-189.
Segklia, A., Seuntjens, E., Elkouris, M., Tsalavos, S., Stappers, E., Mitsiadis, T.A., Huylebroeck, D., Remboutsika, E., and Graf, D. (2012). Bmp7 regulates the survival, proliferation, and neurogenic properties of neural progenitor cells during corticogenesis in the mouse. PLoS One *7*, e34088.
Shitamukai, A., Konno, D., and Matsuzaki, F. (2011). Oblique radial glial divisions in the developing mouse neocortex induce self-renewing progenitors outside the germinal zone that resemble primate outer subventricular zone progenitors. J Neurosci *31*, 3683-3695.
Suzuki, I.K., Kawasaki, T., Gojobori, T., and Hirata, T. (2012). The temporal sequence of the mammalian neocortical neurogenetic program drives mediolateral pattern in the chick pallium. Dev Cell *22*, 863-870.
Taverna, E., Gotz, M., and Huttner, W.B. (2014). The cell biology of neurogenesis: toward an understanding of the development and evolution of the neocortex. Annu Rev Cell Dev Biol *30*, 465-502.
Wang, X., Tsai, J.W., LaMonica, B., and Kriegstein, A.R. (2011). A new subtype of progenitor cell in the mouse embryonic neocortex. Nat Neurosci *14*, 555-561.
Yamashita, W., Takahashi, M., Kikkawa, T., Gotoh, H., Osumi, N., Ono, K., and Nomura, T. (2018). Conserved and divergent functions of Pax6 underlie species-specific neurogenic patterns in the developing amniote brain. Development *145*.
Yu, F.X., Zhao, B., and Guan, K.L. (2015). Hippo Pathway in Organ Size Control, Tissue Homeostasis, and Cancer. Cell *163*, 811-828.

Figure Legends

Figure 1: SMAD1/5 activity is required for RGC self-amplification during chick cortical neurogenesis.

(A) Cortical neurogenesis in the chick, showing the main cortical progenitor subtypes and their modes of division. (B) Chick PAX6$^+$;TBR2$^-$ RGCs and TBR2$^+$ IPCs undergo pH3$^+$ mitoses apically (black arrowheads) and basally (white arrowheads) to the VZ, respectively. (C) The active, phosphorylated form of SMAD1/5/8 (pSMAD1/5/8) immunoreactivity at E5, and (D) its mean intensity ± s.d. measured in 276 apical and 93 basal mitoses obtained from 5 embryos. (E) The pSMAD1/5/8 immunoreactivity in mitotic cortical progenitors 24 hours after *in ovo* electroporation (IOE) with the pTis21:RFP reporter along with a control H2B-GFP-producing plasmid, and (F) its mean intensity ± s.d quantified in 137 pTis21:RFP$^+$ neurogenic divisions and 107 pTis21:RFP$^-$ self-amplifying divisions derived from 8 electroporated embryos. (G-N) The mean proportion ± s.d. of electroporated (H2B-GFP+) cortical progenitors undergoing neurogenic pTis21:RFP+ divisions (white arrowheads) after IOE of shRNA plasmids targeting cSmad1 or cSmad5 (sh-S1/5) or their control (G, H) or IOE of a constitutively active SMAD5 mutant (5-S/D) or its control (K, L), obtained from 8-12 embryos per experimental condition. The mean proportion ± s.d. of PAX6+/-;TBR2+/- and SOX2+/-;HuC/D+/- cells among electroporated (H2B-GFP+) cells 48 hours after IOE of sh-S1/5 (I, J), 5-S/D (M, N) or their respective controls, obtained from 8-20 embryos per experimental condition. Significance was assessed with the non-parametric Mann–Whitney test (D, F), the two-sided unpaired t-test (H, L) or a two-way ANOVA + Sidak's test (J, N). *P<0.05, **P<0.01, ***P<0.001. Scale bars: 50 µm (B, C, I, M), 10 µm (E, G, K). VZ: ventricular zone. See also Figures S1 and S2.

Figure 2: inhibiting SMAD1/5 activity in mouse neural progenitors causes growth retardation, microcephaly and cortical alterations.

(A) Sagittal sections of the developing mouse dorsal telencephalon showing *mSmad1*, *mSmad5* and *mSmad8* transcripts at E14.5, obtained from Genepaint (https://gp3.mpg.de). (B) The pSMAD1/5/8 immunoreactivity at E13.5 and (C) its mean intensity ± s.d. measured in 144 apical and 64 basal mitoses obtained from 3 mouse E13.5 embryos. (D-H) The postnatal evolution of SmadNes mutant mice and their control littermates (D) in terms of mean postnatal weight ± s.d. (E), brain development (F), mean brain weight ± s.d. (G) and the brain/body weight ratio ± s.d. (H), obtained from 3-12 animals per genotype. (I) Coronal sections of the brain of adult SmadNes mutant mice and their control littermates. (J-L) Mean number of $NeuN^+$ neurons ± s.d. (J), neuronal layer organization (K), mean thickness of the layers ± s.d. (L) and the mean number of neurons ± s.d. in the different layers (M) in radial units (100 µm) of the mature cerebral cortex of SmadNes mutant mice and their control littermates, obtained from 3-4 animals per genotype. Significance was assessed with the non-parametric Mann–Whitney test (C, J) or a two-way ANOVA + Sidak's test (E, G, H, L, M). *P<0.05, **P<0.01, ***P<0.001. Scale bars, 50 µm (B), 100 µm (A, K), 500 µm (I). See also Figure S3.

Figure 3: inhibiting SMAD1/5 activity in mouse cortical progenitors causes premature neurogenesis and depletion of the RGC and IPC pools.

(A) Timeline of cortical neurogenesis and BrdU injections during mouse embryonic development. (B-J) Immunostaining and quantification of the mean numbers ± s.d. of $PAX6^{+}$;$TBR2^{-}$ RGCs and $TBR2^{+}$ IPCs (B-D), the neuronal output (% of $BrdU^{+}$; $Tuj1^{+}/BrdU^{+}$ cells, E, F), the generation of early-born $TBR1^{+}$ (G, H) and late-born $SATB2^{+}$ (I, J) cortical excitatory neurons quantified per radial unit (100 µm) in the developing cerebral cortex of SmadNes mutant mice and their control littermates at early (E11.5), middle (E13.5) and late (E17.5) embryonic stages, obtained from 3-5 embryos per genotype and stage. The normality was tested using the values of individual sections. Significance was assessed with the two-sided unpaired t-test (C, D, F, H, J). *P<0.05, **P<0.01, ***P<0.01. Scale bars, 50 µm. CP: cortical plate, IZ: intermediate zone, SVZ: sub-ventricular zone, VZ: ventricular zone. See also Figure S4.

Figure 4: Transcriptional program regulated by SMAD1/5 in early mouse cortical RGCs.

(A) Methodology used to compare the transcriptome of cortical RGCs from SmadNes mutant and control E12.5 embryos. (B) Spearman rank correlation and heat map representing the differentially expressed transcripts (DETs, with a p Adj<0.05) between mutant and control cortical RGCs. (C, D) Representation of the top 10 gene ontology biological processes (C) and transcription factor binding motifs (D) associated with the DETs (with a p Adj<0.1). See also Table S1.

Figure 5: SMAD1/5 regulate early cortical neurogenesis through YAP.

(A) Expression of YAP during early mouse corticogenesis (E11.5), relative to SMAD1/5 activity (pSMAD1/5/8). (B,C) The mean intensity ± s.d. of endogenous YAP (B) and pSMAD1/5/8 (C) immunoreactivity was quantified in 70 apical and 28 basal $pH3^{+}$ mitotic nuclei, obtained from 3 embryos. (D) The correlation between the intensity of endogenous pSMAD1/5/8 and YAP immunoreactivities was assessed by calculating the Pearson's correlation coefficient r. (E) Immunostaining of the developing chick cerebral cortex for total YAP 24 hours after IOE with a control or sh-S1/5 plasmid and (F) its mean ratio ± s.d. quantified in electroporated relative to non-electroporated mitotic cells obtained from 7 embryos (Ctrl: 147 $pH3^{+}$;GFP^{+} cells and 154 $pH3^{+}$;GFP^{-} cells, sh-S1/5: 162 $pH3^{+}$;GFP^{+} cells and 140 $pH3^{+}$;GFP^{-} cells). (G) Immunostaining of pYAP and total YAP and (H) the quantification of the pYAP/YAP intensity ratio ± s.d. in the developing cerebral cortex of E11.5 SmadNes mutant embryos and control littermates, obtained from 4 embryos (12 sections) per genotype. The normality was tested using the values of individual sections. (I-M) Immunostaining and the mean proportion ± s.e.m. of $SOX2^{+/-}$;$HuC/D^{+/-}$ cells (I, J), RGCs ($PAX6^{+}$;$TBR2^{-}$ cells, K), $TBR2^{+}$ cells (L) and ectopic $SOX2^{+}$ cells (M) among electroporated (GFP^{+}) cells 48 hours after IOE of a wild type YAP1 construct (YAP) together with sh-S1 or its control, obtained from n=8-9 embryos per condition. Significance was assessed with the non-parametric Mann–Whitney test (B, C, F), the two-sided unpaired t-test (H) or a two-way ANOVA + Tukey's multiple comparisons test (J-M). *P<0.05, **P<0.01, ***P<0.001. Scale bars, 50 µm. See also Figure S5.

Materials and Methods

Animals

Smad1$^{wt/fl}$;Smad5$^{wt/fl}$;Nestin:Cre$^{+/0}$ embryos and postnatal mice were obtained by crossing *Smad1$^{fl/fl}$;Smad5$^{fl/fl}$* mice with transgenic mice that express Cre-recombinase in neural progenitor cells and somites from E8.5 (*NesCre8* mice: (Moya et al., 2012; Petersen et al., 2002). Smad1$^{wt/fl}$;Smad5$^{wt/fl}$;Nestin:Cre$^{0/0}$ littermates were used as controls. The days of the vaginal plug and birth were defined as E0.5 and P0, respectively. *Smad1$^{fl/fl}$;Smad5$^{fl/fl}$* and *NesCre8* mice were maintained in their original genetic backgrounds. All the experimental procedures were carried out in accordance with the European Union guidelines (Directive 2010/63/EU) and the followed protocols were approved by the ethics committee of the Parc Científic de Barcelona (PCB).

Fertilized white Leghorn chicken eggs were provided by Granja Gibert, rambla Regueral, S/N, 43850 Cambrils, Spain. Eggs were incubated in a humidified atmosphere at 38°C in a Javier Masalles 240N incubator for the appropriate duration and staged according to the method of Hamburger and Hamilton (HH: Hamburger and Hamilton, 1951). According to EU animal care guidelines, no IACUC approval was necessary to perform the experiments described herein, considering that the embryos used in this study were always harvested at early stages of embryonic development. Sex was not identified at these stages.

In ovo electroporation

Unilateral *in ovo* electroporations were performed in the developing chick dorsal telencephalon at stage HH18 (E3, 69-72 hours of incubation). Analyses were performed specifically in the dorsal-medial-lateral region of the developing chick cerebral cortex to minimize any possible variability along the medial-lateral axis. Plasmids were diluted in

RNAse-free water at the required concentration [0 to 4 µg/µl] and injected into the right cerebral ventricle using a fine glass needle. Electroporation was triggered by applying 5 pulses of 50 ms at 22.5 V with 50 ms intervals using an Intracel Dual Pulse (TSS10) electroporator. Electroporated chicken embryos were incubated back at 38°C and recovered at the times indicated.

Plasmids

Inhibition of *cSmad1* and *cSmad5* expression was triggered by electroporation of short-hairpin constructs inserted into the pSuper (Oligoengine) or pSHIN vectors together with a control H2B-GFP-producing plasmid as previously reported (Kojima et al., 2004; Le Dreau et al., 2018; Le Dreau et al., 2012). Electroporation of 2-4 µg/µl of these constructs caused a specific and reproducible 50% inhibition of the target expression (Le Dreau et al., 2012). The pCAGGS_SMAD5-SD_ires_GFP, its control pCAGGS_ires_GFP (pCIG), as well as the pTis21:RFP reporter used to assess the modes of divisions undergone by spinal progenitors, were previously described in details (Le Dreau et al., 2012; Megason and McMahon, 2002; Saade et al., 2013). The pCAGGS_Flag-YAP1_ires_GFP construct was obtained by subcloning from a pCDNA:Flag-YAP1 kindly provided by Conchi Estaras (Levy et al., 2008).

In situ hybridization

Chicken embryos were recovered at the indicated stages, fixed overnight at 4 ºC in 4% paraformaldehyde (PFA), rinsed in PBS and processed for whole mount RNA *in situ* hybridization following standard procedures. Probes against chick *Smad1* (#chEST899n18) and *Smad8* (#chEST222h17) were purchased from the chicken EST project (UK-HGMP RC). Probe against *cSmad5* was kindly provided by Dr Marian

Ros. Hybridized embryos were post-fixed in 4% PFA and washed in PBT, and 45 µM-thick vibratome sections (VT1000S, Leica) were mounted and photographed under a microscope (DC300, Leica). The data show representative images obtained from 3 embryos for each stage and probe. The images of *mSmad1, mSmad5 and mSmad8* expression in the developing mouse dorsal telencephalon at E14.5 were obtained from the Genepaint database (https://gp3.mpg.de).

Histology and Immunohistochemistry

Mouse embryos were recovered at the indicated stages and their heads fixed by immersion in 4% PFA for 24 hours at 4 ºC, cryoprotected with 30% sucrose in PBS, embedded in Tissue-Tek O.C.T. (Sakura Finetek), frozen in isopentane at -30 ºC and sectioned coronally on a cryostat (Leica). Cryosections (14 µm) were collected on Starfrost pre-coated slides (Knittel Glasser) and distributed serially. Postnatal and adult mice were deeply anesthetized in a CO_2 chamber and trans-cardially perfused with 4% PFA. The brains were removed, post-fixed and cryoprotected as indicated above and cryotome (40 µm) sections were then distributed serially. Chicken embryos were carefully dissected, fixed for 2 hours at room temperature (RT) in 4% PFA, rinsed in PBS and cryoprotected with 30% sucrose in PBS and 16 µm-thick coronal sections prepared with a cryostat.

For both species, immunostaining was performed following standard procedures. After washing in PBS containing 0.1% Triton X-100 (PBT), the sections were blocked for 1 hour at RT in PBT supplemented with 10% bovine serum albumin (BSA). When necessary, sections were submitted to an antigen retrieval treatment before blocking by boiling sections for 10 min in sodium citrate buffer (2 mM citric acid monohydrate, 8 mM tri-sodium citrate dihydrate, pH 6.0). For BrdU immunostaining, sections were

incubated before blocking in 50% formamide in 2X SSC at 64 ºC for 10 min followed by an incubation in 2N HCl at 37 ºC for 30 min and finally 10 min in 0.1 M boric acid (pH 8.5) at RT. Sections were then incubated overnight at 4 ºC with the appropriate primary antibodies (Table S2) diluted in a solution of PBT supplemented with 10% BSA or sheep serum. After washing in PBT, sections were incubated for 2 hours at RT with the appropriate secondary antibodies diluted in PBT supplemented with 10% BSA or sheep serum. Alexa488-, Alexa555- and Cy5-conjugated secondary antibodies were obtained from Invitrogen and Jackson Laboratories. Sections were finally stained with 1 µg/ml DAPI and mounted in Mowiol (Sigma-Aldrich).

Cell cycle exit assay

Pregnant female mice received an intra-peritoneal injection of BrdU (100 mg/kg; Sigma) and were sacrificed 24 hours later. Embryos were collected and processed as described above. Sections were immunostained for BrdU and Tuj1 and the cell cycle exit rate (neuronal output) was estimated by quantifying the proportion of $BrdU^+$-immunolabelled cells that were $Tuj1^+$ (% of $Tuj1^+$;$BrdU^+$/$BrdU^+$ cells).

Image acquisition and treatment

Optical sections of mouse and chick embryo fixed samples (coronal views) were acquired at RT with the Leica LAS software, in a Leica SP5 confocal microscope using 10x (dry HC PL APO, NA 0.40), 20x (dry HC PL APO, NA 0.70), 40x (oil HCX PL APO, NA 1.25-0.75) or 63x (oil HCX PL APO, NA 1.40-0.60) objective lenses. Maximal projections obtained from 2µm Z-stack images were processed in Photoshop CS5 (Adobe) or ImageJ for image merging, resizing and cell counting. Optical sections of postnatal and adult mouse samples were acquired with a Leica AF7000 motorized

wide-field microscope. Cell counting in embryo, postnatal and adult mouse samples were performed in a 100 or 200 μm-wide radial column of the lateral cortical wall, as indicated in the figures. Cell counts were performed in a minimum of 3 sections of the same rostral-caudal level per embryo or postnatal mouse sample. Quantification of pSMAD1/5/8, PAX6, TBR2, YAP and pYAP intensities was assessed using the ImageJ software. Cell nuclei of mitotic $pH3^+$ cells or $H2B\text{-}GFP^+$ electroporated and neighboring non-electroporated cells were delimitated by polygonal selection, and the mean intensity was quantified as mean gray values.

Western blot

Total protein extracts (≈ 40 μg) were resolved by SDS-PAGE following standard procedures and transferred onto a nitrocellulose membrane (Hybond-ECL, Amersham Biosciences) that was probed with the primary antibodies (Table S2) whose binding was detected by infra-red fluorescence using the LI-COR Odyssey IR Imaging System V3.0 (LI-COR Biosciences).

Purification of mouse Prominin1$^+$ RGCs

The purification of $Prominin1^+$ cortical RGCs was achieved by fluorescence-activated cell sorting (FACS) of dissociated cells obtained from the forebrain of $Smad1^{wt/fl}$;$Smad5^{wt/fl}$;$Nestin:Cre^{+/0}$ and $Smad1^{wt/fl}$;$Smad5^{wt/fl}$;$Nestin:Cre^{0/0}$ E12.5 embryos. Forebrains of littermates with the same genotype were pooled and incubated in Hanks' balanced salt solution (HBSS) containing 0.6% Glucose and 5 mM EDTA for 5 min at 37 ºC. Cells were mechanically dissociated by gentle trituration and collected by centrifugation at 300 g for 10 min at 4 ºC. Cells were resuspended in 200 μl of incubation media (PBS containing 0.6% glucose, 2% foetal bovine serum and 0.02%

NaN_3) and kept for 10 min at 4 ºC with mild agitation. Cells were then incubated for 30 min at 4 ºC with an APC-conjugated anti-Prominin1 antibody (eBioscience, #17-1331-81) diluted at 0.2 mg/ml. Incubation with a rat IgG1-APC antibody was performed in parallel to define non-specific fluorescence. After the incubation, cells were centrifuged at 300 g for 10 min at 4 ºC and incubated with 1 ml of incubation media. Dissociated cells were then filtered through a falcon tube with a cell strainer cap (BD Biosciences; BD falcon 12 x 75 mm) in which the filter was previously dampened with 500 µl of incubation media. The number of isolated cells was determined using a Neubauer chamber and cells were diluted to a final concentration of 2-3 x 10^6 cells/ml. DAPI (20 ng/mL: Vector Labs) was added to identify dead cells. Sorting was performed with a BD FACS Aria^{TM} Fusion (BD Biosciences) cytometer. After sorting, collector tubes were centrifuged at 1000 g for 10 min at 4 ºC and cell pellets stored at -80 ºC.

RNA-sequencing

RNA was extracted from pools of 6 x 10^5 FACS-isolated cells using the miRNeasy Micro Kit (Qiagen). Quantification of total RNA was performed by Qubit® RNA BR Assay kit (Thermo Fisher Scientific) and RNA 6000 Nano Bioanalyzer 2100 Assay (Agilent) was used to estimate the total RNA integrity. The 3 pairs of samples of RNAs from SmadNes mutant and control RGCs presenting the best RNA integrity were used for sequencing. Sample preparation protocol for the RNASeq libraries was following the manufacturer's recommendations of KAPA Stranded mRNA-Seq Illumina® Platforms Kit (Roche-Kapa Biosystems). The libraries were sequenced on HiSeq2500 (Illumina) in paired-end mode with a read length of 2 x 100 bp using TruSeq SBS Kit v4 (Illumina). Each sample was sequenced in a fraction of a sequencing v4 flow cell lane, following the manufacturer's protocol. Image analysis, base calling and quality

scoring of the run were processed using the manufacturer's software Real Time Analysis (RTA 1.18.66.3) and followed by generation of FASTQ sequence files.

RNA-Seq paired-end reads were mapping against *Mus musculus* reference genome (GRCm38) using STAR version 2.5.3a (Dobin et al., 2013) with ENCODE parameters for long RNA. Isoforms were quantified using RSEM version 1.3.0 (Li and Dewey, 2011) with default parameters for stranded sequencing and the gencode version M15. Differential isoform analysis was performed with DESeq2 version 1.18 (Love et al., 2014) with default parameters. We considered differentially expressed transcripts those showing a *p*-adjusted value < 0.05 or *p*-adjusted value <0.1 (extended list). Fold-change (FC) values between genotypes (SmadNes mutants over controls) are expressed in Log2 (Table S1). The GO term enrichment analysis (biologic process) of the extended DET signature was performed with the PANTHER classification system (http://pantherdb.org) and the Transfac/Jaspar analysis using Enrichr (Chen et al., 2013; Kuleshov et al., 2016).

Statistical analyses

No statistical method was used to predetermine sample size. The experiments were not randomized. The investigators were not blinded to allocation during experiments. Statistical analyses were performed using the GraphPad Prism 6 software (GraphPad Software, Inc.). Unless noted otherwise (see quantifications), cell counts were typically performed on 3-5 images per embryo and *n* values correspond to different embryos or animals. The normal distribution of the values was assessed by the Shapiro-Wilk normality test. Significance was then assessed with a two-sided unpaired t-test, one-way ANOVA + Tukey's test or two-way ANOVA + Sidak's or Tukey's test for data presenting a normal distribution, or alternatively with the non-

parametric Mann–Whitney test for non-normally distributed data. The following convention was used: n.s, non-significant; *P<0.05, **P<0.01, ***P<0.001. The detailed information related to quantifications are detailed in the figure legends.

Supplemental items

Figure S1 (related to Figure 1): Neurogenesis and expression of *cSmad1/5/8* during chick cerebral cortex development.

Figure S2 (related to Figure 1): inhibiting and increasing SMAD1/5 activity in chick cortical RGCs respectively forces and restrains their progression towards neuronal commitment and differentiation.

Figure S3 (related to Figure 2): Reduction in SMAD1/5 protein levels, brain size and cortical layer alterations in the SmadNes mutant mice.

Figure S4 (related to Figure 3): Absence of patterning defects and of cell cycle alterations in the cerebral cortex of SmadNes mutant embryos.

Figure S5 (related to Figure 5): SMAD1/5 regulate early cortical neurogenesis through YAP.

Table S1 (related to Figure 4): List of differentially expressed transcripts between cortical RGCs from SmadNes mutant and control E12.5 embryos.

Table S2: List of primary antibodies.

Supplemental Information

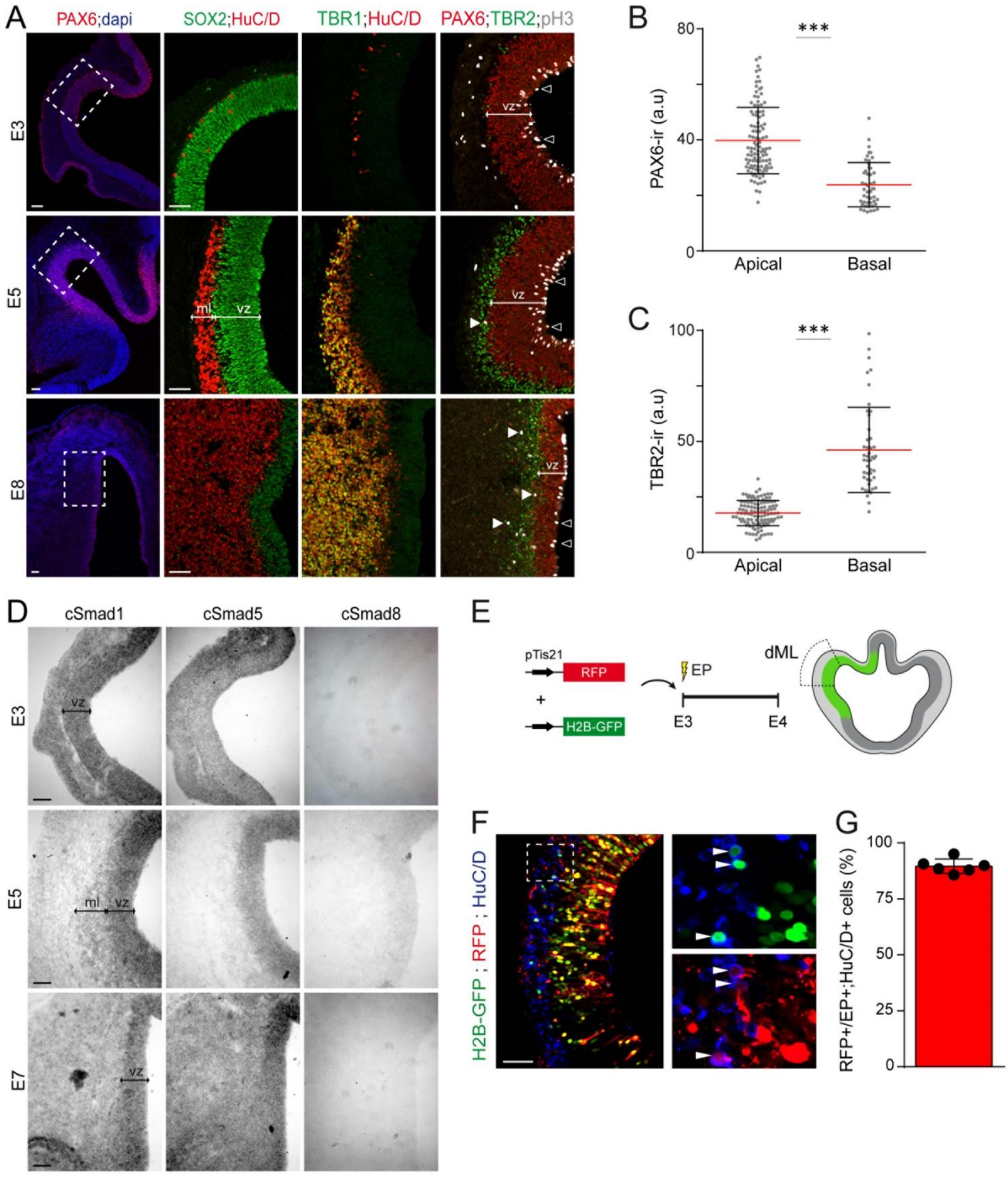

Figure S1

Figure S1 (related to Figure 1): Neurogenesis and expression of *cSmad1/5/8* during chick cerebral cortex development.

(A) Coronal telencephalic sections from 3, 5 and 8 days-old chick embryos showing the developing $PAX6^+$ cerebral cortex, formed of $SOX2^+$ neural progenitors that populate the germinal ventricular zone (VZ) while the first differentiating HuC/D^+ and $TBR1^+$ neurons migrate basally to form the mantle layer (ML). Neural progenitors from the developing chick cerebral cortex can be subdivided in two different subpopulations: the $PAX6^+$;$TBR2^-$ radial glial cells (RGCs) that undergo mitosis at the apical surface ($pH3^+$;$PAX6^+$, black arrowheads) and the $TBR2^+$ intermediate progenitor cells (IPCs) that divide mostly basally from E5 onwards ($pH3^+$;$TBR2^+$, white arrowheads). (B, C) The mean intensity ± s.d of endogenous PAX6 (B) and TBR2 (C) immunoreactivity was quantified in mitotic ($pH3^+$) nuclei of 108 apical and 48 basal cortical progenitors obtained from 5 chick E5 embryos. (D) Coronal sections showing *cSmad1*, *cSmad5 and cSmad8* transcripts detected by *in situ* hybridization in the developing cerebral cortex of E3, E5 and E7 chick embryos. (E-G) The activity of the pTis21:RFP reporter was assessed during cortical neurogenesis 24 hours after in ovo electroporation (IOE) of the dorsal telencephalon of E3 chick embryos. (F) Representative image of pTis21:RFP^+ cells among the electroporated (H2B-GFP^+) cells that differentiated into HuC/D^+ neurons 24 hours later and (G) its quantification, presenting the mean proportion and individual values of RFP^+ cells among H2B-GFP^+;HuC/D^+ cells ± s.d obtained from 6 electroporated embryos. Significance was assessed with the non-parametric Mann–Whitney test (B,C). ***P<0.001. Scale bars: 50 µm. VZ: ventricular zone, ML: mantle layer.

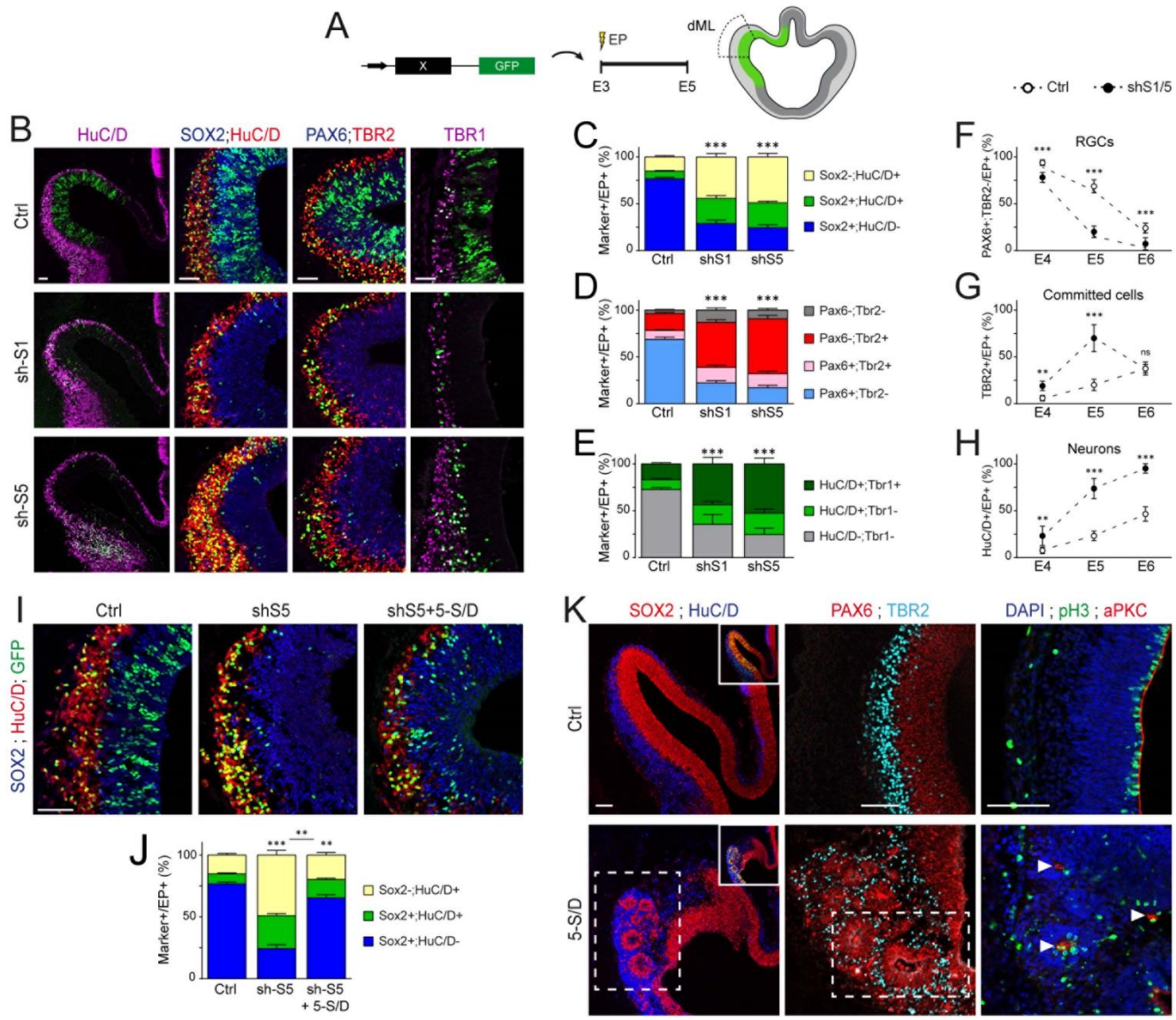

Figure S2

Figure S2 (related to Figure 1): inhibiting and increasing SMAD1/5 activity in chick cortical RGCs respectively forces and restrains their progression towards neuronal commitment and differentiation.

(A) *In ovo* electroporation (IOE) of the chick dorsal telencephalon. (B-H) SMAD1/5 activity was inhibited at E3 by IOE of sh-RNA plasmids targeting *cSmad1* (sh-S1), *cSmad5* (sh-S5) or their control (Ctrl) together with a plasmid producing H2B-GFP. (B) Representative images and (C-E) mean proportions ± s.e.m of $SOX2^{+/-}$;$HuC/D^{+/-}$ (C), $PAX6^{+/-}$;$TBR2^{+/-}$ (D) and $HuC/D^{+/-}$;$TBR1^{+/-}$ (E) cells among electroporated (H2B-GFP^{+}) cells, assessed 48 hours after IOE with sh-S1, sh-S5 or their control and obtained from 5-13 embryos per experimental condition. (F-H) The mean proportion ± s.d of $PAX6^{+}$;$TBR2^{-}$ (RGCs, F), $TBR2^{+}$ (committed cells, G) and HuC/D^{+} (Neurons, H) cells among electroporated (H2B-GFP^{+}) cells were assessed 24 (E4), 48 (E5) and 72 (E6) hours after IOE and obtained from 6-20 embryos per condition and stage. (I) Representative images and (J) mean proportion ± s.e.m of $SOX2^{+/-}$;$HuC/D^{+/-}$ cells among electroporated (H2B-GFP^{+}) cells 48 hours after IOE of a control plasmid, or sh-S5 combined with a control plasmid or with the constitutively active SMAD5-S/D mutant (5-S/D), obtained from 8-13 embryos per condition. (K) Representative images showing that IOE of SMAD5-S/D can cause the abnormal generation of ectopic rosettes of $SOX2^{+}$ cortical progenitors. The $PAX6^{+}$ and $TBR2^{+}$ cells forming these rosettes developed an ectopic apical-basal polarity, as revealed by immunostaining for the apical marker atypical PKC (aPKC, arrowheads), and divide mostly at the center of the rosettes ($pH3^{+}$). Significance was assessed with a two-way ANOVA + Sidak's test (C-H) or a two-way ANOVA + Tukey's test (J). **P<0.01; ***P<0.001. Scale bars: 50 µm.

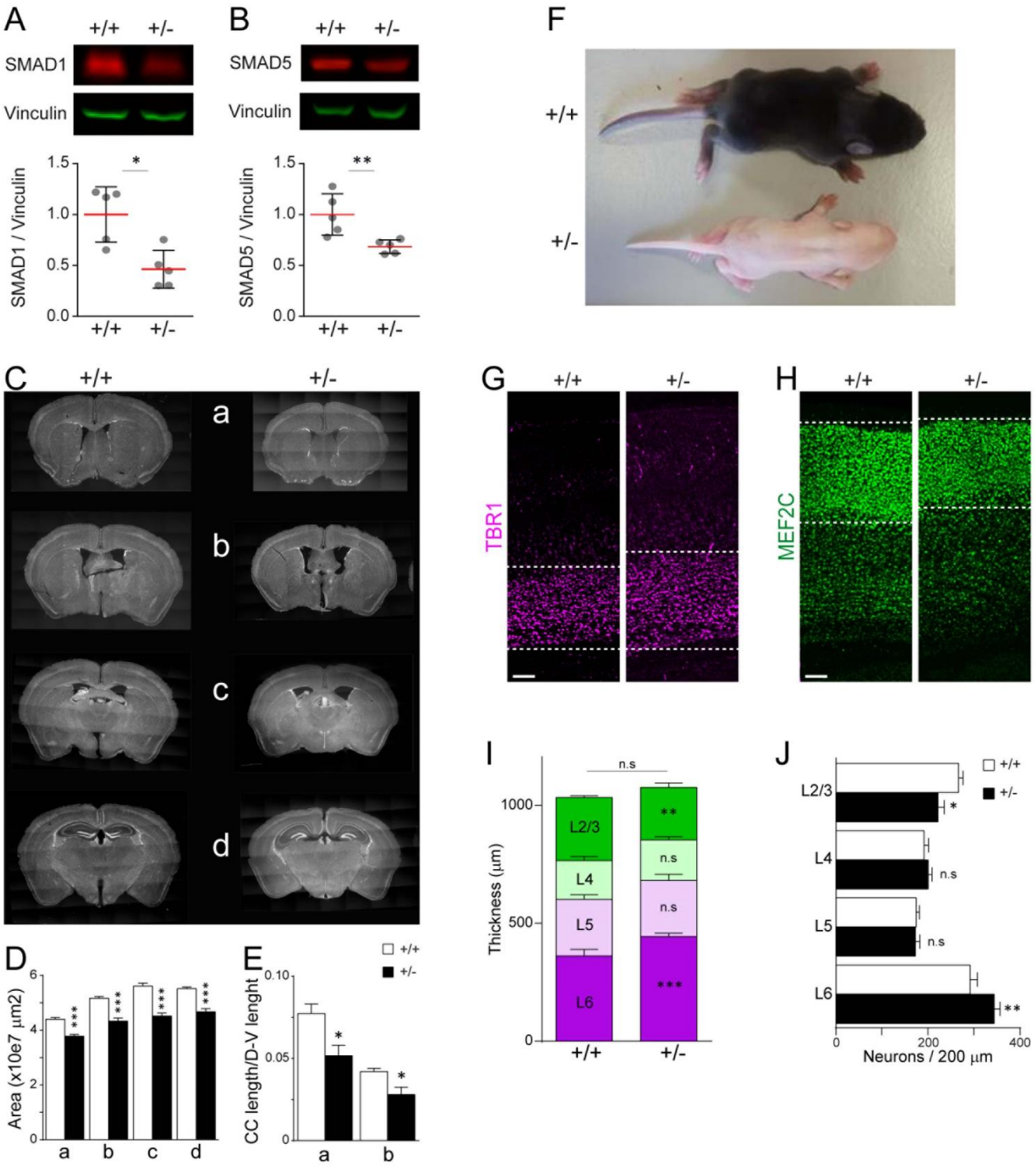

Figure S3

Figure S3 (related to Figure 2): Reduction in SMAD1/5 protein levels, brain size and cortical layer alterations in the SmadNes mutant mice.

(A-B) The levels of SMAD1 (A) and SMAD5 (B) proteins were assessed by Western blot in extracts obtained from telencephalons of E11.5 SmadNes mutant embryos (+/-) and control littermates (+/+), relative to the levels of Vinculin. The data represent the mean ratio ± s.d obtained from 5 mutant embryos and 5 control littermates. (C) Representative images of the adult brain of SmadNes mutant mice (+/-) and their control littermates (+/+) in 4 different positions along the rostral-caudal axis (a to d, from rostral to caudal) and (D) their mean area ± s.e.m, obtained from 3-5 embryos per genotype. (E) The thickness of the corpus callosum of the adult brain of SmadNes mutants and control littermates was measured in coronal sections in 2 different positions (a and b) along the rostral-axis, relative to whole dorsal-ventral (D-V) length. The data represent the mean ratio ± s.e.m obtained from 5 control and 3 mutant mice. (F) SmadNes mutant mice (+/-) and their control littermates (+/+) at postnatal day 7 (P7). (G, H) Representative images of (G) early-born $TBR1^+$ L6 and (H) late-born $SATB2^+$ L4-2/3 projection neurons in the developing cerebral cortex of the SmadNes mutant pups and their control littermates. (I, J) The mean thickness ± s.e.m (I) and mean number of neurons per layer ± s.e.m (J) in a 200 µm-wide radial column unit of the cerebral cortex of SmadNes mutants (n= 5) and control littermates (n= 6) at P7. Significance was assessed with the non-parametric Mann–Whitney test (A, B, E and I for the total cumulated thickness) or a two-way ANOVA + Sidak's test (D, I, J). *P<0.05, **P<0.01, ***P<0.001. Scale bars: 500 µm (C), 100 µm (G, H).

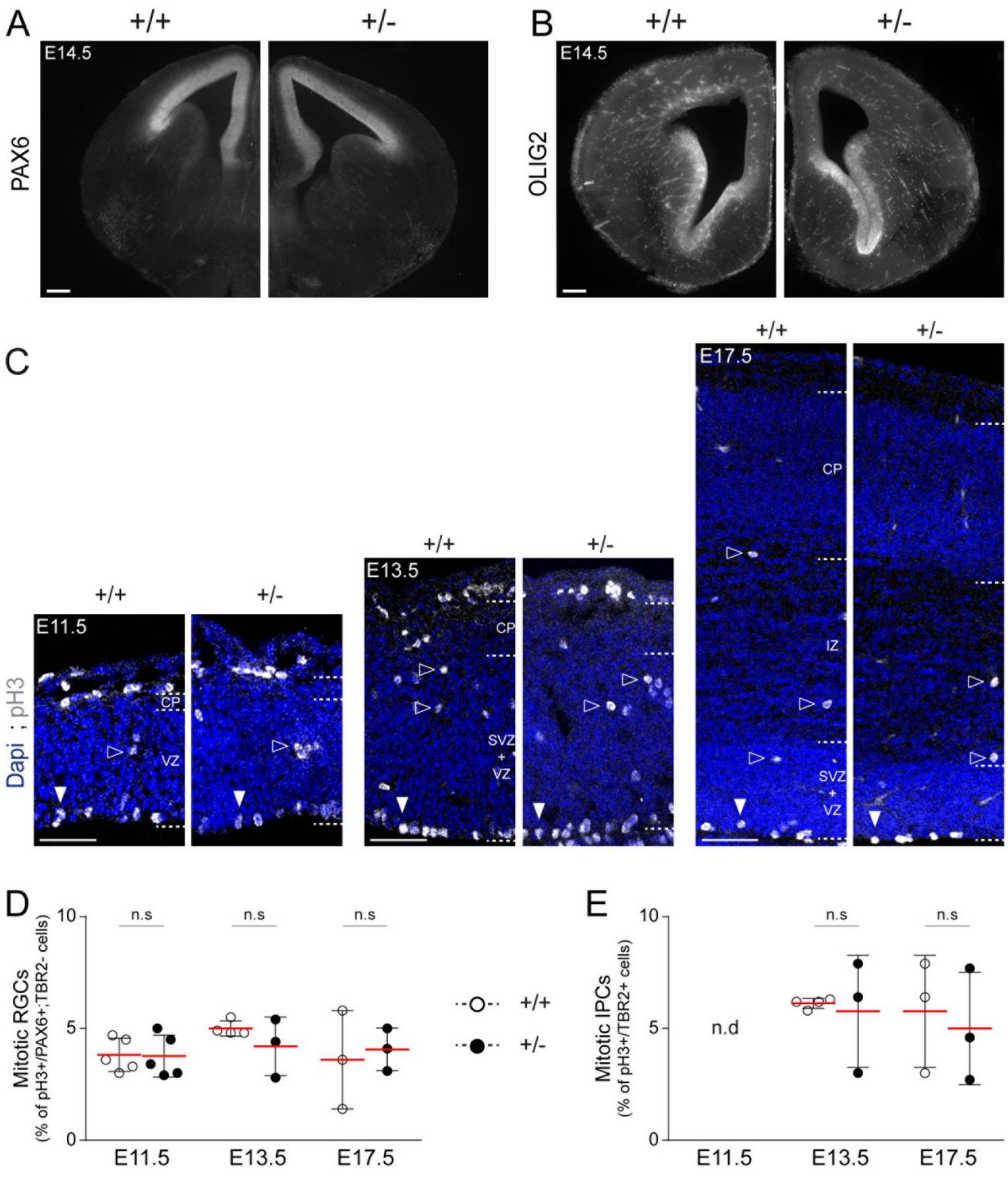

Figure S4

Figure S4 (related to Figure 3): Absence of patterning defects and of cell cycle alterations in the cerebral cortex of SmadNes mutant embryos.

(A, B) Coronal sections showing PAX6 (A) and OLIG2 (B) immunostaining in the telencephalon of E14.5 SmadNes mutant embryos (+/-) and control littermates (+/+). No obvious alteration in the expression domains of these pallial (PAX6) and sub-pallial (OLIG2) patterning markers was observed in the telencephalon of the SmadNes mutant embryos. (C) Coronal sections showing apical (white arrowheads) and basal (black arrowheads) $pH3^+$ mitoses in the developing cerebral cortex of SmadNes mutant embryos (+/-) and control littermates (+/+) at E11.5, E13.5 and E17.5. (D, E) The data represent the mean proportion ± s.d of (D) $pH3^+/PAX6^+;TBR2^-$ cells (mitotic RGCs) and (E) $pH3^+/TBR2^+$ cells (mitotic IPCs) counted in a 100 µm-wide radial column unit of the developing cerebral cortex of SmadNes mutant and control littermates embryos, obtained from 3-5 embryos per genotype and stage. The normality was tested using the values of individual sections. Significance was assessed at each developmental stage with the two-sided unpaired t-test. NS: not significant. nd: not determined. Scale bars, 100 µm (A, B), 50 µm (C). CP: cortical plate, IZ: intermediate zone, SVZ: sub-ventricular zone, VZ: ventricular zone.

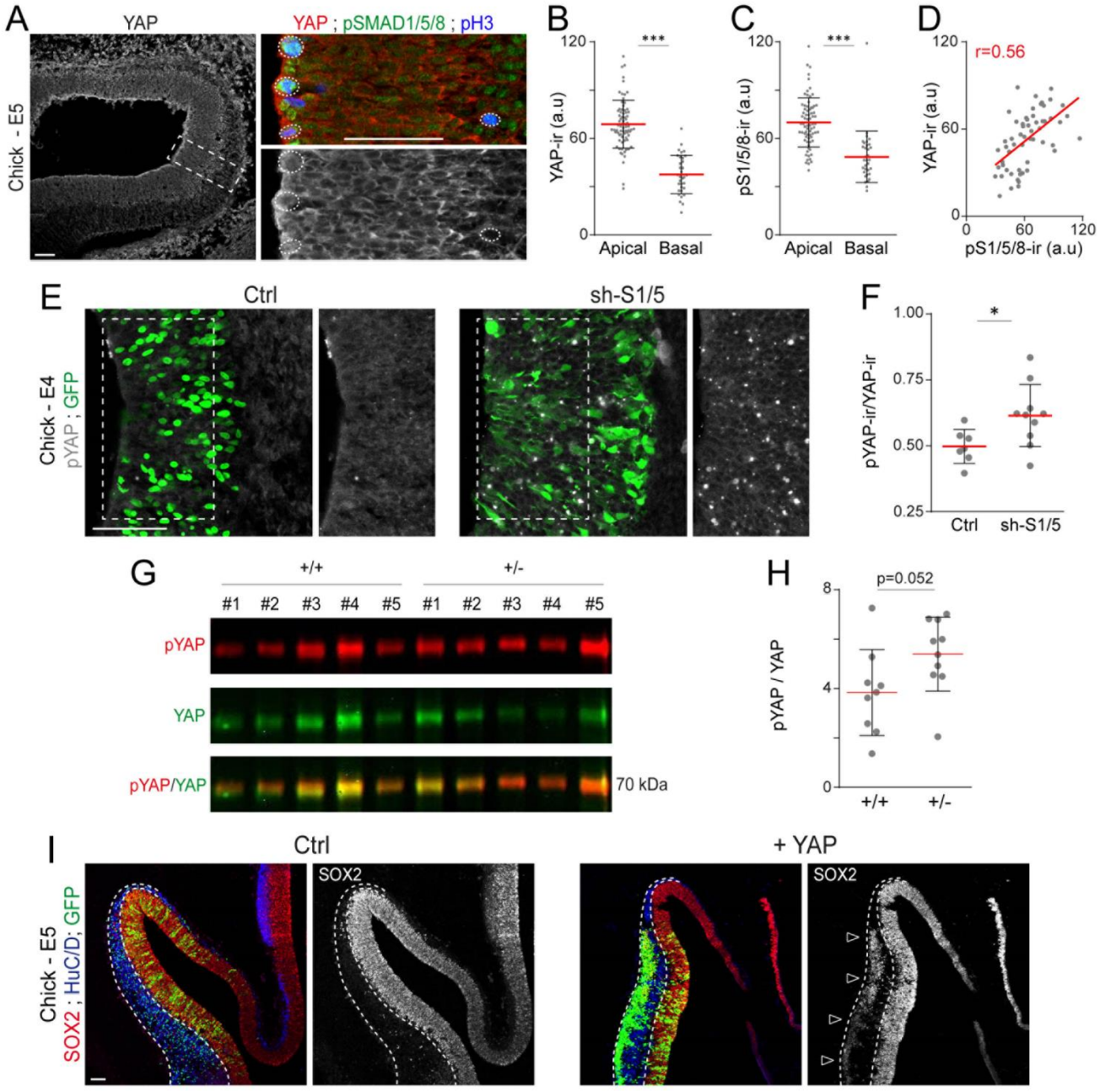

Figure S5

Figure S5 (related to Figure 5): SMAD1/5 regulate early cortical neurogenesis through YAP.

(A) Expression of YAP during chick corticogenesis, relative to SMAD1/5 activity (pSMAD1/5/8). (B,C) The mean intensity ± s.d of endogenous YAP (B) and pSMAD1/5/8 (C) immunoreactivity was quantified in 74 apical and 33 basal mitotic ($pH3^+$) nuclei obtained from 3 chick E5 embryos. (D) The correlation between the intensity of endogenous pSMAD1/5/8 and YAP immunoreactivities was assessed by calculating the Pearson's correlation coefficient r. (E) Immunostaining of the form of YAP phosphorylated at Serine 123 (pYAP) and (F) quantification of the mean ratio ± s.d of pYAP/YAP intensity obtained 24 hours after IOE with sh-S1/5 (10 sections from 3 embryos) or its control (7 sections from 3 embryos). (G) Western blot detection of the levels of pYAP and total YAP in extracts obtained from telencephalons of E11.5 SmadNes mutant embryos (+/-) and control littermates (+/+). (H) Quantification of the mean pYAP/YAP ratio ± s.d, obtained from 10 SmadNes mutant embryos (+/-) and 9 control littermates (+/+) derived from 2 different litters. (I) Immunostaining of the developing chick cerebral cortex for $SOX2^+$ neural progenitors and HuC/D^+ differentiating neurons 48 hours after IOE with a construct overexpressing the wild type form of YAP (YAP) or a control, showing that YAP overexpression can lead to a massive ectopic delamination of SOX2+ electroporated cells in the basal part of the mantle zone. Significance was assessed with the non-parametric Mann–Whitney test (B, C, F), the two-sided unpaired t-test (D, H).*P<0.05, **P<0.01, ***P<0.001. Scale bars, 50 µm.

Table S2: List of primary antibodies

REAGENT or RESOURCE	**SOURCE**	IDENTIFIER
Antibodies		
anti-aPKC (mouse)	Santa Cruz Biotechnologies	Cat #SC-17781 (H-1) RRID:AB_628148
anti-BrdU (rat)	AbD Serotec	Cat #MCA2060 RRID:AB_323427
anti-pHistone3 (rat)	Sigma Aldrich	Cat #H9908 RRID:AB_260096
anti-HuC/D (mouse)	Life Technologies	Cat #A-21271 RRID:AB_221448
anti-MEF2c (rabbit)	Abcam	Cat#ab64644 RRID:AB_2142861
anti-NeuN (mouse)	Millipore	Cat # MAB377 RRID: AB_2298772
anti-OLIG2 (rabbit)	Millipore	Cat#AB9610 RRID: AB_570666
anti-PAX6 (mouse)	DSHB	Cat#pax6 RRID:AB_528427
anti-PAX6 (rabbit)	Covance / Biolegend	Cat #901301 RRID:AB_2565003
anti-Prominin1 (rat)	eBioscience	Cat #17-1331-81 RRID: AB_823120
anti-SMAD1 (rabbit)	Cell Signaling Technologies	Cat #6944S RRID:AB_10858882
anti-SMAD5 (rabbit)	Cell Signaling Technologies	Cat # 12534S RRID: n.d
anti-pSMAD1/5/8 (rabbit)	Cell Signaling Technologies	Cat#9511 RRID:AB_331671
anti-SOX2 (rabbit)	Abcam	Cat #ab97959 RRID:AB_2341193
anti-TBR1 (rabbit)	Abcam	Cat #ab31940 RRID:AB_2200219
anti-TBR2 (rabbit)	Abcam	Cat #ab23345 RRID:AB_778267
anti-TUBULIN-b3 (Tuj1) (mouse)	Covance	Cat #MMS-435P RRID:AB_2313773
anti-Vinculin (mouse)	Sigma	Cat # V9131 RRID: AB_477629
anti-YAP (mouse)	Santa Cruz Biotechnologies	Cat # sc-101199 RRID:AB_1131430
anti-pYAP (rabbit)	Cell Signaling Technologies	Cat#4911 RRID:AB_2218913